Original paper

Cassiterite in granite, granitic pegmatites, greisen and hydrothermal veins, the Bugarura–Kuluti Nb–Ta–Sn deposit, Karagwe–Ankole Belt, Rwanda: petrography and chemical composition

Jakub RYZNAR[1*], Jaroslav PRSEK[1], Adam WŁODEK[1], Benjamin HEREDIA[2], Tonny B. THOMSEN[2], Pavel UHER[3]

[1] *CAGH University of Science and Technology. Postal address: AGH University Building A0, room 06, al. Mickiewicza 30, 30-059 Krakow, Poland; jakub.ryznar@proxis.pl*
[2] *Geological Survey of Denmark and Greenland. Postal address: Øster Voldgade 10 1350 Copenhagen K Denmark*
[3] *Department of Mineralogy, Petrology and Economic Geology, Faculty of Natural Sciences, Comenius University. Postal address: Ilkovičova 6, 842 15 Bratislava, Slovakia*
** Corresponding author*

This study provides detailed mineralogical, textural and compositional features of cassiterite from the Bugarura–Kuluti Nb–Ta–Sn deposit located in the Mezoproterozoic Karagwe–Ankole Belt of eastern Rwanda. The cassiterite occurs within two-mica, peraluminous "tin" granites, lithium–caesium–tantalum (LCT) pegmatites, greisens, and hydrothermal quartz–muscovite veins. The cassiterite from quartz–muscovite veins exhibit progressive oscillatory zonation and contains rutile and ilmenite inclusions. The chemical signature of the vein cassiterite is marked by elevated Ti and low Ta, Nb and Fe concentrations. The cassiterite from the pegmatites and associated greisens contains numerous Ta–Nb oxide inclusions. Both types expose complex and patchy textures, often associated with younger generations of cassiterite. Contrary to cassiterite from quartz–muscovite veins, the pegmatitic/greisen cassiterite has elevated Ta, Nb and Fe and low Ti contents. The cassiterite from the granite is anhedral, exhibits irregular patchy textures, and lacks zonation. Mineral inclusions in the two-mica granite cassiterite were not observed. In comparison to cassiterite from veins, greisens and pegmatites, granitic cassiterite is characterised by chemical compositions showing intermediate concentrations of minor and trace elements. The origin of Sn mineralisation involves segregation of rare lithophile elements into residual pegmatite melts and hydrothermal fluids and their crystallization in Sn and Nb–Ta minerals in LCT pegmatites and quartz veins. The majority of the cassiterite in pegmatites precipitated during the process of greisenisation by circulating aqueous solutions, probably exsolved from pegmatite melts. Most of hydrothermal fluids, enriched with volatiles and Sn, used tectonic fractures to escape farther to adjacent metasedimentary rocks allowing for the generation of quartz–muscovite veins by interaction with country rocks and/or mixing with meteoric waters.

Keywords: cassiterite, Karagwe–Ankole Belt, Sn metallogeny, tin granites
Received: 18 May 2023; accepted: 20 July 2024; handling editor: J. Cempírek
The online version of this article (doi: 10.3190/jgeosci.389) contains electronic supplementary material.

1. Introduction

The Bugarura–Kuluti mining district (formerly Bugalula–Kuruti), located in the eastern part of Rwanda, is known for its tin and tantalum mineralisation. The Mesoproterozoic rocks forming this region belong to the Western Domain of the Karagwe–Ankole Belt (KAB), which together with its coeval southwest counterpart, i.e., the Kibara Belt (KIB) (Fig. 1), forms one of the world's largest Ta–Nb–Sn–W provinces (e.g., Varlamoff 1972; Fernandez–Alonso et al. 2012; Melcher et al. 2015; Hulsbosch 2019). Metasedimentary rocks of both the KIB and KAB were intruded by three main granites generations, viz. G1–G3, G4 and G5 (Kokonyangi et al. 2004; Tack et al. 2010; Dewaele et al. 2011; Nambaje et al. 2020). The two youngest generations, called G4 yield an age of 986 ± 10 Ma, whilst G5 yield an age of 614 ± 9 Ma, both being parental granites for Nb–Ta–Sn–W mineralisation. Mineral deposits emplaced in the Karagwe–Ankole Belt (KAB) include quartz–muscovite hydrothermal veins, lithium–caesium–tantalum (LCT) pegmatites with associated greisen, and secondary eluvial and alluvial deposits (Varlamoff 1972; Dewaele et al. 2011; Pohl et al. 2013; Hulsbosch 2019). Although all the above-mentioned deposits are found in the Bugarura–Kuluti (BK) area and form one continuous mineral system, no comprehensive studies of the BK mineralisation have been carried out so far, and therefore the processes leading to their formation are poorly understood.

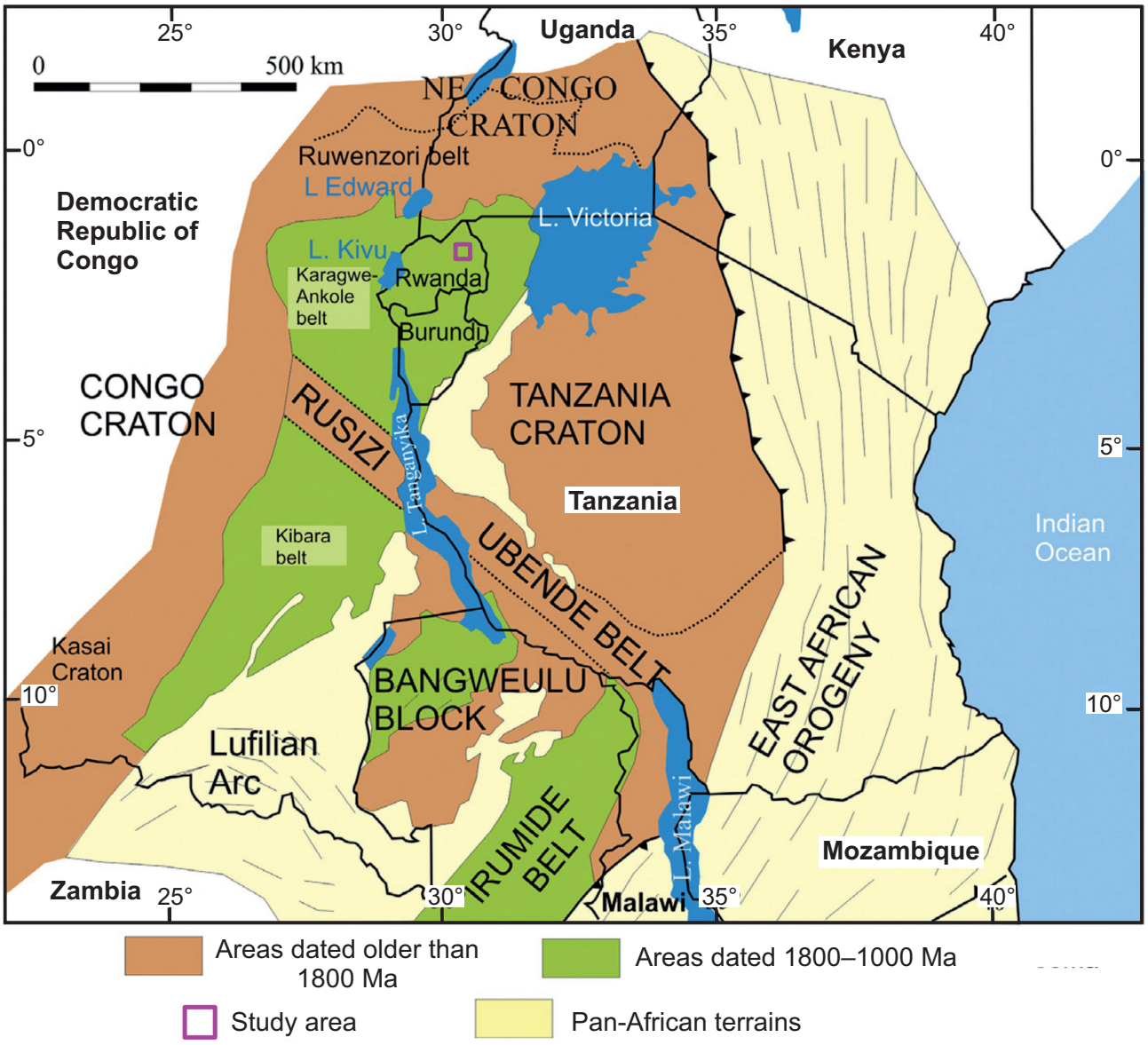

Fig. 1 General geological setting of the Karagwe–Ankole Belt and the Kibara Belt. Modified after Dewaele et al. (2011).

Cassiterite is the principal tin ore mineral occurring in several granite-related deposits including disseminated magmatic mineralisation in granites, mineralisation in late-magmatic pegmatites, and mineralisation in magmatic–hydrothermal or metasomatic deposits (among others e.g., Dewaele et al. 2016a; Moscati and Neymark 2020; Zoheir et al. 2020). Cassiterite can accommodate a variety of trace elements including Fe, Mn, Ti, W, Nb, Ta, Zr, Hf, V, Cr, U, and Sc (e.g., Schneider et al. 1978; Cheng et al. 2019). The enrichment of these elements in cassiterite depends on various factors including the chemical composition and nature of mineralising fluids and melts, but also the host rocks (Möller et al. 1988; Cheng et al. 2019; Nambaje et al. 2020). The relationship between Fe + Mn and Nb + Ta in the cassiterite may reflect its origin (e.g., Tindle and Breaks 1998; Pieczka et al. 2007). Moreover, the distribution and concentration of redox-sensitive elements, such as W, U, Fe and Sb, together with textural studies may explain the redox conditions of fluids and mineral precipitation processes (Cheng et al. 2019).

In this study, we examine cassiterite from different ore styles from the BK metallogenic district of eastern Rwanda. The examined deposits are considered as being

⇨

Fig. 2 Geological map of the Karagwe–Ankole Belt (KAB) with location of study area. The most important granite-related ore deposits of Rwanda are indicated. B: Bugarama; Bu: Bugarura; ED: eastern domain; G: Gifurwe; GG: Gatumba-Gitarama; Ka: Kabaya; Ku: Kuluti; L: Rutsiro; M: Mwaka; MN: Musha–Ntunga; N: Nyakabingo; R: Rutongo; Rw: Rwinkwavu; WD: western domain. Modified after Hulsbosch (2019).

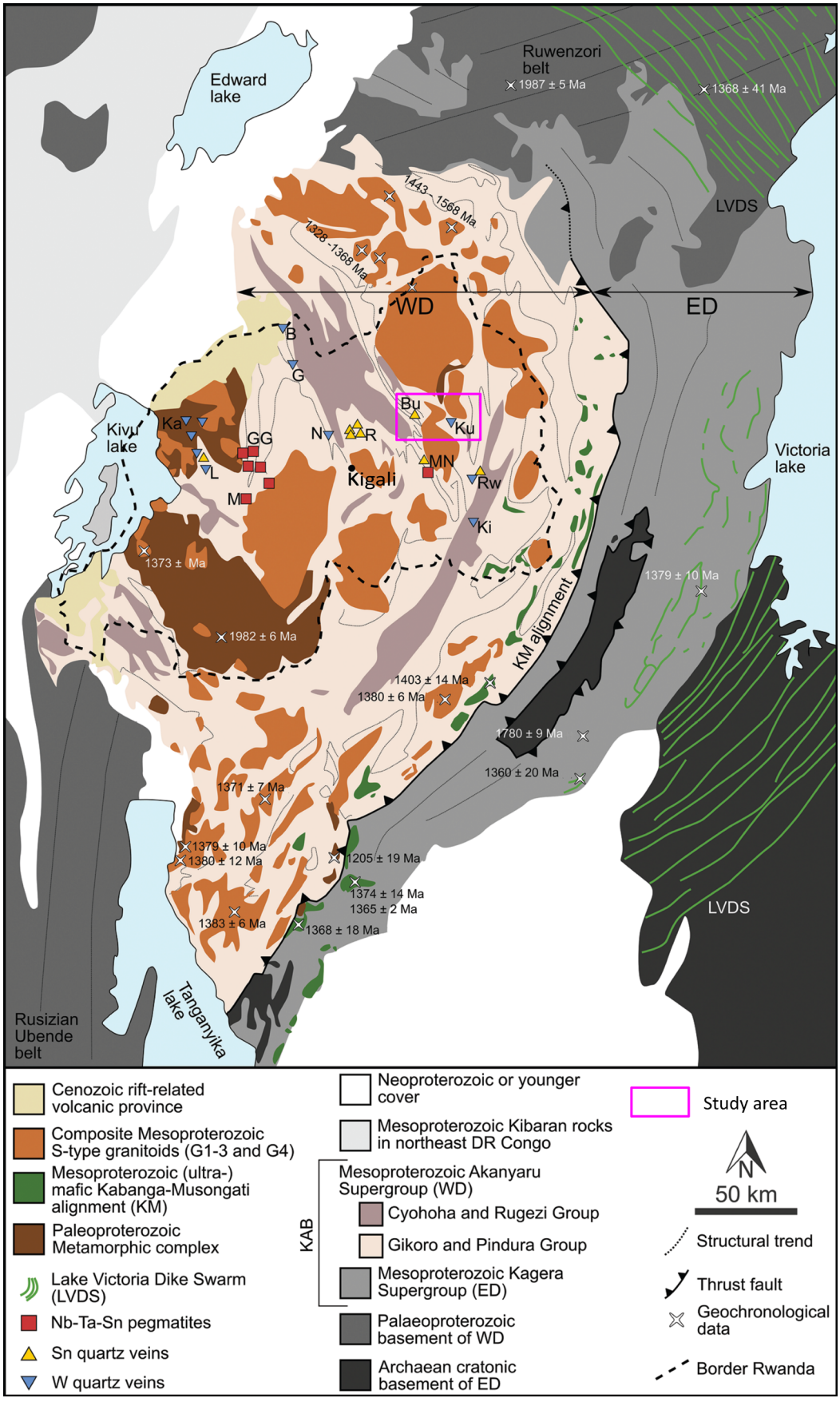
Edward lake
Ruwenzori belt
1987 ± 5 Ma
1368 ± 41 Ma
1443 - 1568 Ma
1328 - 1368 Ma
LVDS
WD
ED
B
G
Bu
Ku
Ka
Kivu lake
GG
N
R
MN
Rw
L
M
Kigali
Ki
Victoria lake
1373 ± Ma
1379 ± 10 Ma
1982 ± 6 Ma
KM alignment
1403 ± 14 Ma
1380 ± 6 Ma
1780 ± 9 Ma
1360 ± 20 Ma
1371 ± 7 Ma
1379 ± 10 Ma
1380 ± 12 Ma
1205 ± 19 Ma
1374 ± 14 Ma
1365 ± 2 Ma
1383 ± 6 Ma
1368 ± 18 Ma
LVDS
Tanganyika lake
Rusizian Ubende belt
Cenozoic rift-related volcanic province
Composite Mesoproterozoic S-type granitoids (G1-3 and G4)
Mesoproterozoic (ultra-) mafic Kabanga-Musongati alignment (KM)
Paleoproterozoic Metamorphic complex
Lake Victoria Dike Swarm (LVDS)
Nb-Ta-Sn pegmatites
Sn quartz veins
W quartz veins
Neoproterozoic or younger cover
Mesoproterozoic Kibaran rocks in northeast DR Congo
KAB
Mesoproterozoic Akanyaru Supergroup (WD)
Cyohoha and Rugezi Group
Gikoro and Pindura Group
Mesoproterozoic Kagera Supergroup (ED)
Palaeoproterozoic basement of WD
Archaean cratonic basement of ED
Study area
N
50 km
Structural trend
Thrust fault
Geochronological data
Border Rwanda

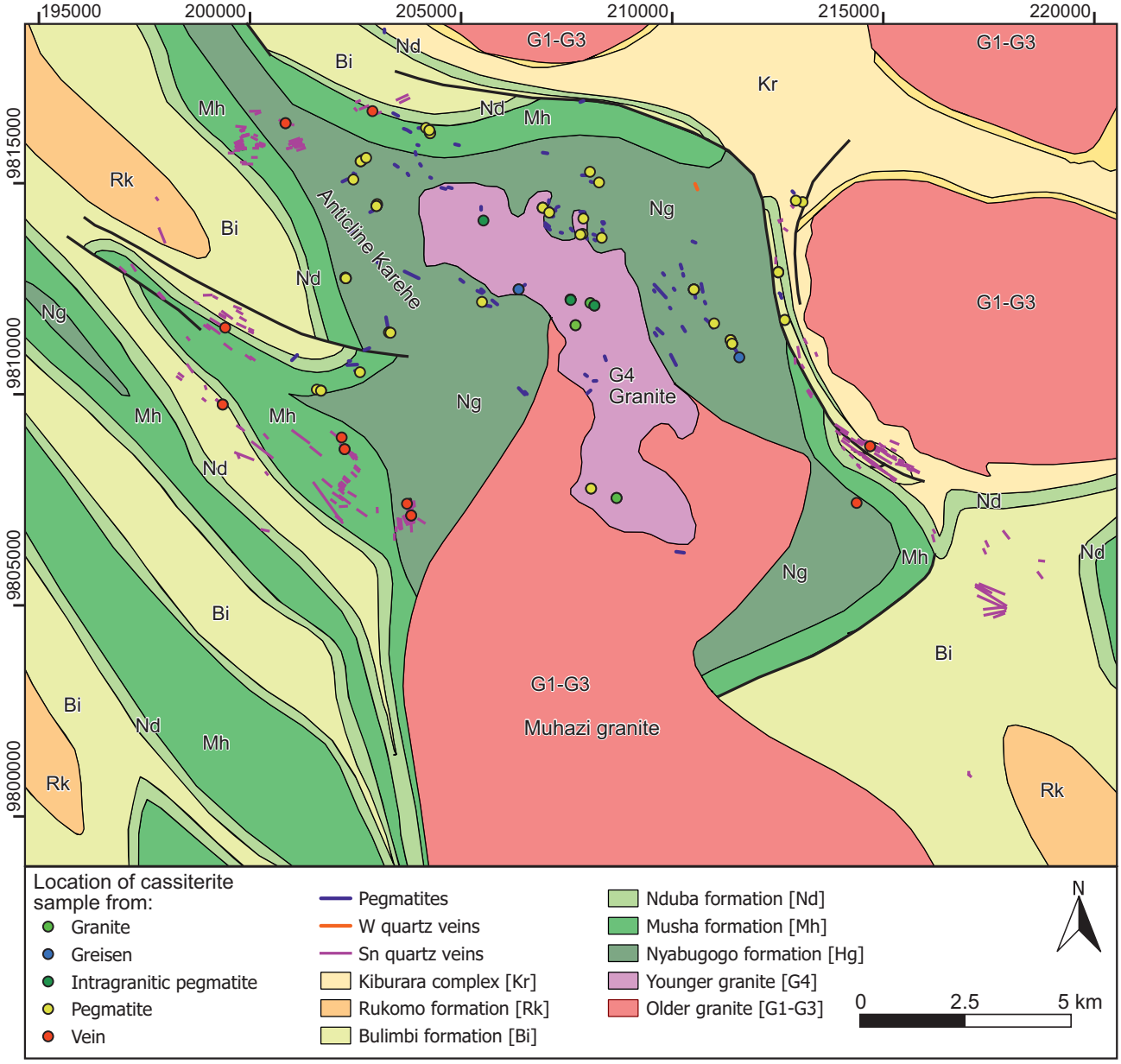

Fig. 3 Geological setting of Bugarura and Kuluti with location of cassiterite samples. All rock formations refer to metasedimentary rocks of the Mezoproterozoic Karagwe–Ankole Belt. Modified after Hanon and Rusanganwa (1991). Coordinates in UTM36S.

connected as one system and thus provide an excellent case study to compare and track the chemical and physical characteristics of cassiterite from the source up to the farthermost primary occurrence. Microscopy studies and electron probe microanalysis (EPMA) analysis were used to characterise cassiterite composition in detail. We focus especially on interpretation of cassiterite chemical composition and textures, to understand its precipitation mechanisms. The objective of this paper is to provide further insights into the ore genesis in the Kibara metallogenic province and to underline the potential of cassiterite as a petrological–geochemical tool for understanding of the evolution of Sn-mineralizing systems. To achieve that, our primary targets were studies of (1) the major and trace elemental concentrations and the substitution mechanisms in cassiterite; (2) the compositional zoning and correlations between micro-textures and trace elemental abundances in cassiterite; (3) the origin of cassiterite mineralisation.

2. Geological setting of the Karagwe–Ankole Belt

The Karagwe–Ankole Belt (KAB) stretches from the eastern part of the Democratic Republic of Congo,

through Rwanda, Burundi to the western part of Tanzania (Fig. 1). It has been formed and developed between the Archean to Paleoproterozoic Congo Craton and the Tanzania–Bangweulu Block (Fernandez–Alonso et al. 2012; Debruyne et al. 2015). The southern border of the orogen is marked by the Paleoproterozoic Rusizi Belt, which divides the KAB from its coeval counterpart the Kibara Belt (KIB).

The Mezoproterozoic Karagwe–Ankole Belt mainly consists of siliciclastic metapelite and meta-arenite turbidite sequences filling two structurally separated basins, namely the Western Domain and Eastern Domain (Fernandez–Alonso et al. 2012; Fig. 2). These rocks belong to the Akanyaru Supergroup, which is subdivided into the Gikoro, Pindura, Cyohoha, and Rugezi Groups (Baudet et al. 1988; Fernandez–Alonso et al. 2012). The sedimentary rocks of the KAB underwent a regional low-grade (Barrovian), amphibolite- to greenschist-facies metamorphism (Baudet et al. 1988; Rusanganwa 1988; Van Daele et al. 2020). They were also intruded by Meso- to Neoproterozoic granitoids and subordinate mafic and sub-volcanic rocks (e.g., Tack et al. 2010; Fernandez–Alonso et al. 2012; De Clercq et al. 2021). There are three known generations of A- and S-type granites in the Western Domain, namely G1–G3, G4 and G5. SHRIMP U–Pb in zircon grains from G1–G3 granites yield ages of ca. 1375 ± 5 Ma (Tack et al. 2010), whereas zircons for the G4 granites yield ages at 986 ± 10 Ma (Tack et al. 2010). The youngest G5 granite emplaced at ca. 614 ± 9 Ma ago (Th–Pb monazite; Nambaje et al. 2021). The two last magmatic events are considered to be the source of Sn, Ta–Nb and W mineralisation in the KAB (Tack et al. 2010; Fernandez–Alonso et al. 2012). High degrees of magmatic fractionations of G4 granite magmas led to the formation and emplacement LCT pegmatites hosting Ta–Nb–Sn mineralisation, greisen with Sn, and hydrothermal quartz veins with Sn and/or W mineralisation (e.g., Pohl et al. 2013; Hulsbosch 2019). The G5 granite is the source of the youngest quartz veins with Sn mineralisation (Nambaje et al. 2021).

3. Methodology

3.1. Mapping and sampling

Different localities containing cassiterite were sampled, including nine quartz veins, 20 pegmatites, seven greisens and four granites. Due to the low quantity of ore minerals, granites and pegmatites were crushed and panned to obtain a sufficient amount of heavy concentrate material to carry out the mineralogical study. All mapped mineralised structures are presented in the geological map with their general strike (Fig. 3).

3.2. Analytical methods

Careful microscopic observation was undertaken prior to microanalysis of cassiterite in 28 polished thin sections. Electron microprobe analyses were carried out on distinct lighter and darker zones of cassiterite as identified using transmitted light microscopy.

A total of 801 spot compositions were obtained by electron microprobe, 563 on cassiterite in 161 selected crystals and 238 on their inclusions (212 columbite group mineral, 21 rutile, 5 ilmenite analyses). Back-scattered electron (BSE) images, chemical microanalyses from carbon-coated thin sections and cathodoluminescence images (CL) were performed using a JEOL JXA-8230 Super Probe electron probe micro-analyser (EPMA) equipped with five wavelength-dispersive X-ray spectrometers at the Geology, Geophysics and Environmental Protection department of AGH University of Science and Technology in Krakow, Poland. Standards, analytical X-ray lines used in analytical procedure and element detection limits (wt. %) include diopside (Mg*K*α, 0.04, Ca*K*α, 0.03), albite (Al*K*α, 0.05), metallic scandium (Sc*K*α, 0.05), rutile (Ti*K*α, 0.03), rhodonite (Mn*K*α, 0.06), hematite (Fe*K*α, 0.06), zircon (Zr *L*α, 0.07), cassiterite (Sn*L*α, 0.04), $LiNbO_3$ (Nb*L*α, 0.12), manganotantalite (Ta*L*α, 0.21), and scheelite (W*M*α, 0.09). Analyses were conducted at an accelerating voltage of 15 kV and a beam current of 20 nA with 20 second count times and beam size of 1 μm; ZAF (atomic number, absorption, fluorescence excitation) corrections were applied. Cathodoluminescence imaging was conducted at an accelerating voltage of 15 kV and a beam current of 5 nA.

4. Results

4.1. Geology and mineralisation of the Bugarura–Kuluti area

The BK area is situated in eastern Rwanda, approx. 50 km to the NE from Kigali (Fig. 2). The geology of BK comprises Mesoproterozoic phyllites, metapelites and quartzites of Pindura and Gikoro groups (Baudet et al. 1988) (Fig. 3). At a regional scale, the Bugarura–Kuluti area is situated on flanks of the NW–SE trending Karehe anticline (Hanon and Rusanganwa 1991). It contains numerous second-order folds following the same trend. The core of the anticline was intruded by the two-mica, peraluminous Muhazi granite (Fig. 3). Two main discontinuous structures have been mapped in the region, NW–SE bedding-parallel faults, and E–W to NE–SW oriented faults (Hulsbosch et al. 2017).

The BK presents a characteristic spatial sequence of deposits, composed of centrally located parental granite


a
Alb
Qz
Bt
2 cm
b
Kln
Ms
Qz
20 cm
c
Ms
Pl
Qz
d
Ms
Cst
Qz
3 cm
e
f
Kln
Ms
Qz
20 cm
g
Tur
Qz
Ms
Tur
Ms
50 cm
h
Fe
Cst
Ms
Qz
20 cm

followed by LCT pegmatites and hydrothermal quartz–muscovite veins in the peripheral part of the area (Fig. 3). Greisen developed only in kaolinised and muscovitised pegmatites.

The central part of the area is represented by the Muhazi granite which consists of G1–G3 and G4 granite generations (Fig. 3). The G4 granite was emplaced to the north of the older generation, and it is a medium- to coarse-grained, non-foliated rock, composed of quartz, plagioclase, K-feldspar, biotite and muscovite (Fig. 4a). Accessory minerals are represented by cassiterite, columbite-group minerals (CGM), staurolite, zircon and monazite-(Ce). Pegmatites were emplaced both in the G4 granites and surrounding country rocks. Intragranitic pegmatites form dykes and flat-laying sills up to ~2 m thick. Beside rock-forming mineral like quartz, muscovite and kaolinite (Fig. 4b), they contain traces of CGM, cassiterite, Ti oxides, zircon, monazite and significant amount of tourmaline. Pegmatites in country rocks were emplaced within phyllites of the Karehe anticline. These pegmatites form a structurally controlled swarm emplaced around the granite dome with a maximum radius of ~3 km (Fig. 3). Most of pegmatites are parallel to the bedding of hosting phyllites, following the NW–SE general trend of the Karehe anticline. A minority of them, follow E–W and NE–SW direction. The thicknesses of the pegmatites vary from 1 to 15 m, but most commonly they are 2–3 m thick. Main pegmatite forming minerals include quartz, muscovite and albite while accessory minerals consist of CGM, cassiterite, tourmaline, zircon, Ti oxides and staurolite (Figs 4c, f). Pegmatites emplaced farthest from the granite, located near the hydrothermal veins, contain accessory ilmenite while zircon is absent. The recent research on Ta–Nb oxides indicates that the pegmatites follow Fe–Mn regional fractionation trend towards high Mn/(Mn + Fe) compositions (Ryznar et al. 2023). Pegmatites were variably affected by sodic, potassic, and argillic alteration, while their contact with phyllites is marked by an intensive boron metasomatism marked by large amounts of tourmaline minerals. The upper part of the vertical and subvertical dykes is enriched in Sn, more than Ta–Nb, mineralisation which could indicate vertical zoning of pegmatites. The cassiterite mainly occurs in greisen nests but may also concentrates in kaolinite–quartz–muscovite assemblages. Greisens contain quartz, greenish muscovite, cassiterite and traces of CGM (Fig. 4d).

Hydrothermal quartz–muscovite veins were emplaced in phyllites, metapelites and quartzites in the peripheral parts of the BK (Fig. 3). This zone begins just above pegmatites and continues up to ~8 km from the central part of granite. The veins in phyllites and metapelites are usually concordant to the bedding. They follow NW–SE direction with a steep dip angle of 60–90°. Thickness of the veins reaches 3–5 m; however, most commonly they are 0.6–1.0 m thick. Although the veins do not appear to be significantly affected by younger tectonic processes and that they can be traced for hundreds of meters, their pinch-and-swell structure hampers exploration and mining of these ore bodies. In phyllites and metapelites, mineralised quartz veins might be distinguished from barren ones by the characteristic structure including a quartz core in the central part of the vein and muscovite selvages at the contact with the country rock (Fig. 4g). The country rock at the contact with both barren and mineralised veins is intensively tourmalinised.

Veins in quartzites were emplaced perpendicularly to the bedding, in radial fractures of folds. Similar to the Rutongo deposit, these veins are limited to quartzite beds and form a parallel system of veins occurring close to each other (Dewaele et al. 2009). The thickness of a single vein in quartzites is usually 2 m, but may reach up to 5 m.

Mineral composition of all mineralised veins at BK consists of quartz, muscovite and cassiterite hosting accessory rutile and ilmenite inclusions (Fig. 4h). Some parts of veins may contain goethite and sometimes kaolinite. The cassiterite occurs in nugget-like nests weighing from a few kilograms up to several tones. Larger nests occur in phyllite-hosted veins, however, their distribution is scattered. The cassiterite in quartzite-hosted veins occurs in smaller nests but mineralisation is more evenly distributed throughout the vein. The overall Sn grade in quartz veins in both types of host rocks strongly depends on the amount of muscovite.

⇦

Fig. 4 Representative field photos of cassiterite-hosting rocks from Bugarura–Kuluti area; **a –** the sample of coarse-grained G4 granite, **b –** kaolinised intragranitic pegmatite with brownish muscovite, hosting coarse CGMs, **c –** non-altered, mega-crystalline pegmatite hosting coarse CGM and minor cassiterite, **d –** greisen with greenish muscovite and visible cassiterite crystals, **e –** typical structure of the altered pegmatite with quartz–muscovite greisen (below the hammer) and quartz-muscovite-kaolinite assemblage above, **f –** kaolinite–muscovite–quartz assemblage of the altered pegmatite hosting Sn–Ta–Nb mineralizations, **g –** typical structure of mineralised vein with quartz core, muscovite selvages and tourmaline alteration, **h –** mineral composition of mineralised quartz vein. Cst – cassiterite, Tur – tourmaline, Alb – albite, Bt – biotite, Qz – quartz, Ms – muscovite, Fe – Fe oxides, Kln – kaolinite, Pl – plagioclase.

4.2. Cassiterite

4.2.1. Micro-textures, inclusions and size variations

The size of cassiterite crystals from Bugarura–Kuluti deposits increase away from the granite. In the G4 granite, cassiterite grains are 100–250 μm; in pegmatites, they vary from 500 μm to 3 mm; in greisens the size varies

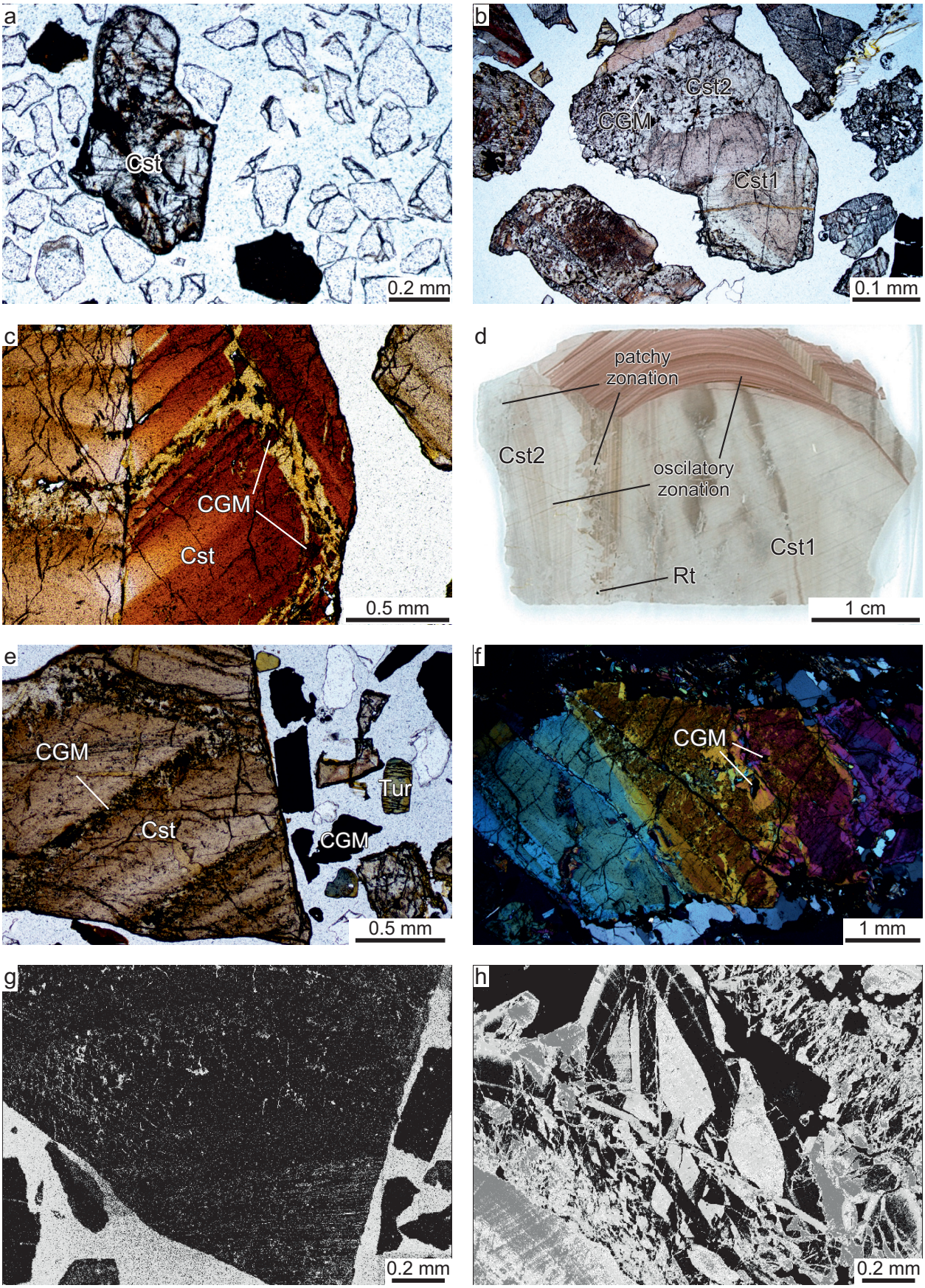
a
Cst
0.2 mm
b
Cst2
CGM
Cst1
0.1 mm
c
CGM
Cst
0.5 mm
d
patchy zonation
Cst2
oscilatory zonation
Cst1
Rt
1 cm
e
CGM
Cst
Tur
CGM
0.5 mm
f
CGM
1 mm
g
0.2 mm
h
0.2 mm

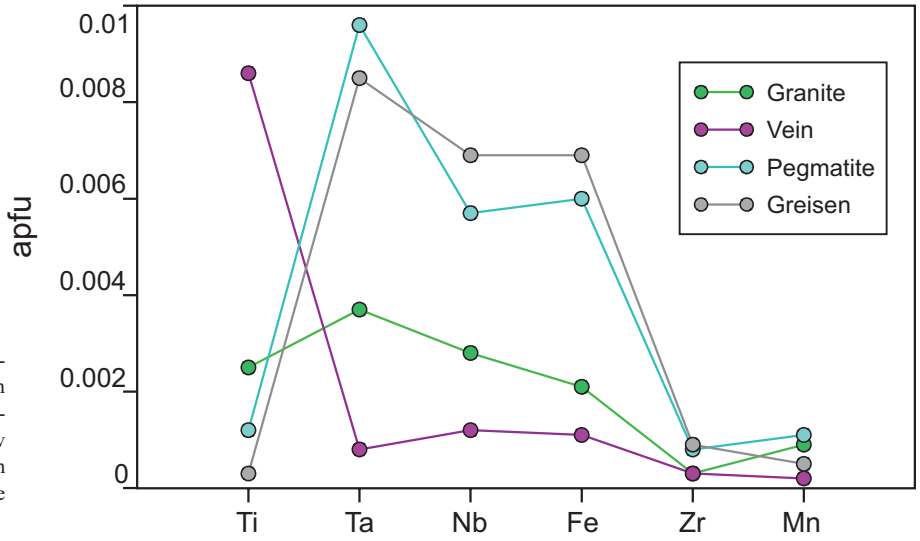

Fig. 6 The average concentration of selected trace elements in cassiterite from different types of deposits. The main difference is observed in high Ti and low Ta + Nb concentrations in quartz vein cassiterite compared to granite, pegmatite and greisen type.

from 0.5 to 3 cm; in hydrothermal quartz veins cassiterite occurs as nuggets reaching several kg up to thousands kg nests, where single crystals are 2–25 cm.

In transmitted light microscopy, the cassiterite exhibits a moderate to intense pleochroism from brownish yellow to dark brown colour, and intense colourful anisotropy (Figs 5c, f). The majority of crystals are anhedral (Figs 5a, b) whereas subhedral crystals have only been observed in the wall zone of pegmatites, corresponding to less than 10 % of the total cassiterite crystals. Some cassiterite crystals from greisen and vein type deposits show oscillatory zoning with darker and lighter parallel bounds not visible in reflected light or backscatter electron images (BSE: Figs 5c, e). However, most of the granite, pegmatite and greisen cassiterite crystals are patchy or sector zoned (Fig. 5b). Cathodoluminescence images of a cassiterite from the pegmatites and greisens poorly show internal zoning (Fig. 5g) while the cassiterite from the quartz veins displays heterogeneous type textures, in which many individual segments have triangular shape (Fig. 5h). Comparison of chemical composition with images suggests that the difference in CL colours could reflect a change in crystal orientation or a subtle chemical change, but not detected by EMPA.

Textural variations in a single crystal indicate different episodes of cassiterite which most probably reflects dissolution–reprecipitation of primary crystals observed in vein-type cassiterite (Fig. 5d). In case of cassiterite from pegmatite and greisen deposits, the last generation is represented by pale or transparent cassiterite phase with abundant CGM inclusions (Fig. 5b). Sometimes, mineral inclusions in oscillatory zoned crystals usually form narrow bands, parallel to the crystal zoning (Fig. 5c). Three types of mineral inclusions have been identified in the cassiterite: (1) columbite-group minerals for pegmatites, greisens and very rarely for quartz veins; (2) ilmenite and (3) rutile for quartz veins.

⇦

Fig. 5 Selected micro-photographs of different cassiterite generations from the Bugarura–Kuluti area; **a –** anhedral crystal of cassiterite from the granite (Plane-Polarised Light – PPL), **b –** typical cassiterite from pegmatites with almost transparent zones enriched in CGM inclusions, **c –** oscillatory texture and intense pleochroic colours of cassiterite from greisen. One parallel to the crystal texture, yellowish bound of cassiterite is highly enriched with CGM inclusions (PPL), **d –** typical zonation of cassiterite from quartz vein. Patchy zonation is formed by partly dissolution – reprecipitation of earlier cassiterite, **e –** oscillatory zonation of cassiterite from pegmatite (PPL), **f –** colourful anisotropic cassiterite from pegmatite with CGM inclusions (Cross-Polarised Light – XPL), **g –** cathodoluminescence image of a cassiterite from picture e), **h –** cathodoluminescence image of a vein-type cassiterite presenting "cracked" texture. Cst – cassiterite, CGM – columbite group minerals, Tur – tourmaline, Qz – quartz, Ms – muscovite, Fe – Fe oxides.

4.2.2. Chemical composition

There are distinct variations in the chemical composition of the cassiterite from different types of deposits from the BK.

The cassiterite from the Muhazi granite has slightly low TiO_2 (0.13 wt. %) concentration whereas Ta_2O_5 (0.54 wt. %), Nb_2O_5 (0.24 wt. %) and FeO (0.10 wt. %) concentrations are in between of the quartz vein and pegmatite cassiterites (Tab. 1; Fig. 6). The cassiterite from pegmatites has high Ta_2O_5 (1.41 wt. %), Nb_2O_5 (0.51 wt. %), FeO (0.29 wt. %) and low TiO_2 (0.07 wt. %) content compared to the granite and cassiterite in the veins (Tab. 1; Fig. 6). The cassiterite from the greisen has similar chemical pattern to the pegmatite cassiterite with high Ta_2O_5 (1.26 wt. %), Nb_2O_5 (0.61 wt. %), FeO (0.33 wt. %) and low TiO_2 (0.02 wt. %) content. Conversely to the greisen and pegmatite type grains, the cassiterite from hydrothermal quartz vein has high TiO_2 (0.46 wt. %) and low Ta_2O_5 (0.12 wt. %), Nb_2O_5 (0.11 wt. %), FeO (0.05

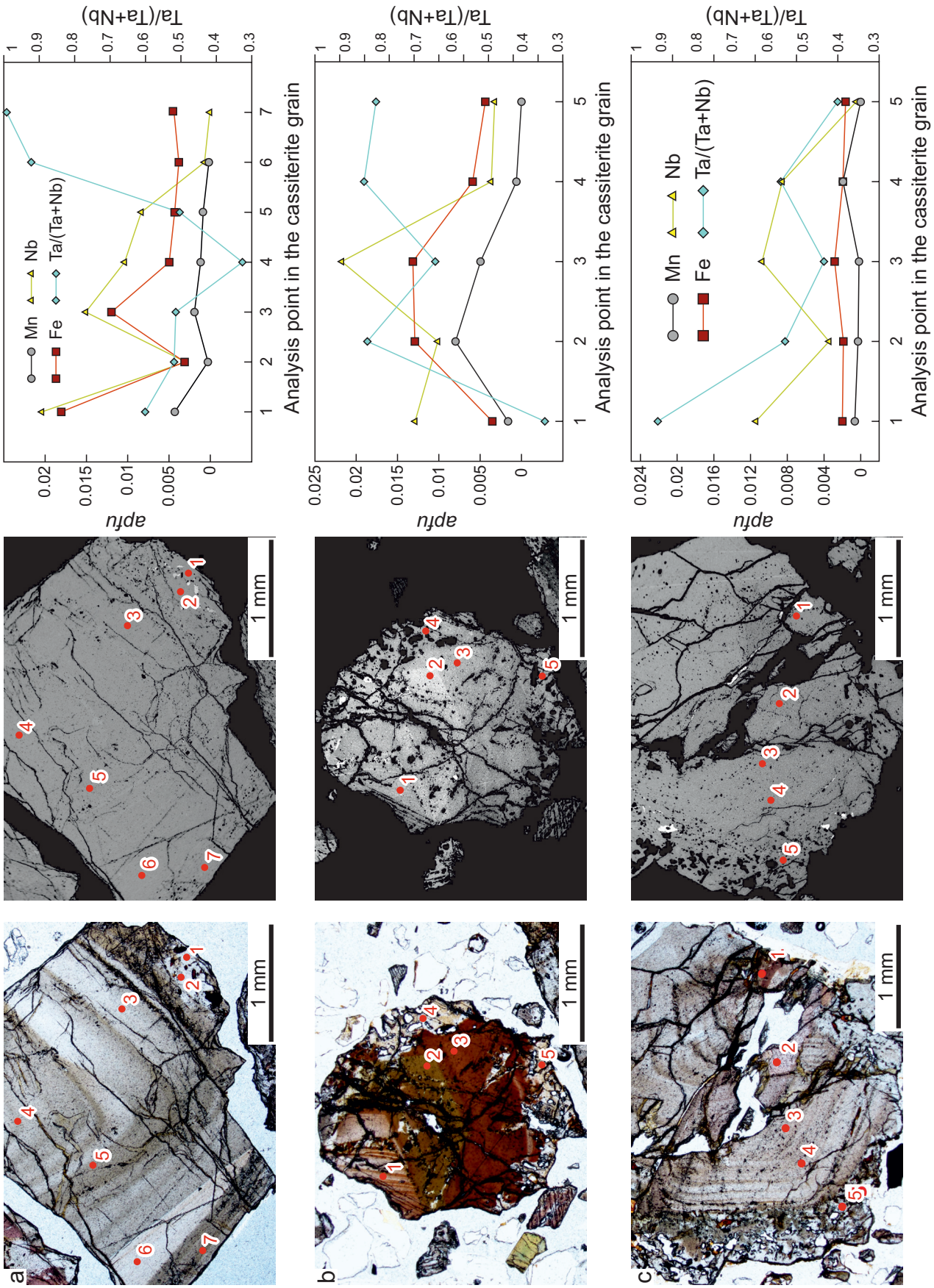
a
b
c
1 mm
apfu
Analysis point in the cassiterite grain
Mn
Fe
Nb
Ta/(Ta+Nb)

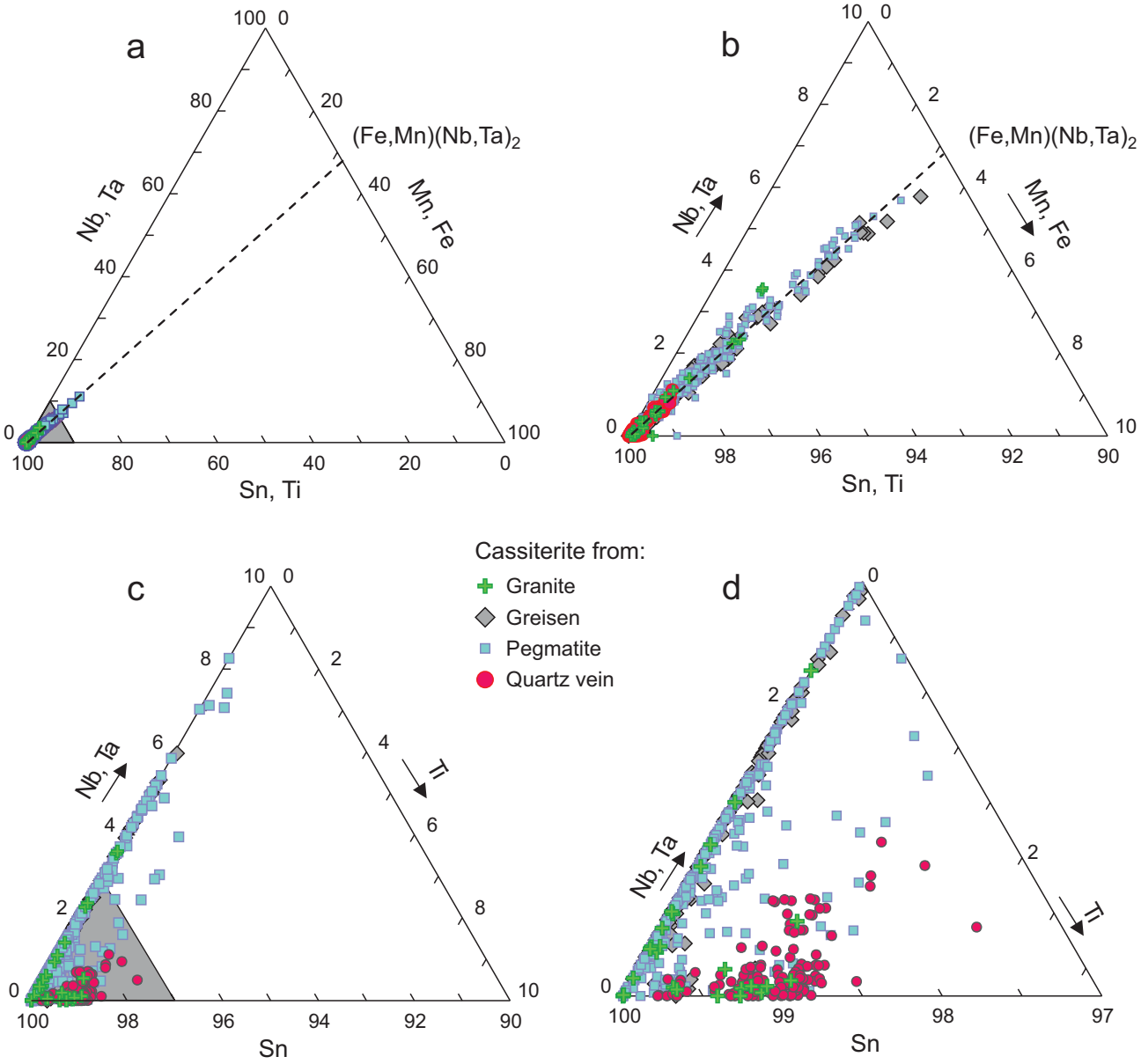

Fig. 8 (Nb,Ta)–(Fe,Mn)–(Sn,Ti) (**a** and **b**), and (Nb,Ta)–Ti–Sn (**c** and **d**) diagrams showing atom ratios of selected elements in cassiterite from granite, greisen, pegmatite and quartz vein-type deposit. Diagram (**b**) represents the detail of (**a**), while diagram (**d**) represents the detail of (**c**).

⇦

Fig. 7 Transmitted light microscopy (PPL) and SEM backscattered images of cassiterite samples from different pegmatites with corresponding contents of selected minor elements in selected spots based on EMPA; **a** – oscillatory texture of cassiterite with darker zones enriched in Fe, Nb and Ta. Increasing Ta/(Ta+Nb) ratio from the centre of the crystal (spot 4) towards the rim (spots 1 and 7) indicates decreasing temperature of the system; **b** – oscillatory and progressive zoning of the cassiterite. Similar trend of increasing Ta/(Ta+Nb) towards the rim. The darkest zone of the crystal corresponds to the highest Nb concentration; **c** – positive Ta/(Ta+Nb) trend towards the rim in oscillatory zoned cassiterite crystal. Later cassiterite generations in all images are characterised by the highest Ta/(Ta+Nb) values and relatively low Fe and Mn concentrations, often corroded texture and increased number of CGM inclusions, e.g. spots 6 and 7 in a), 4 and 5 in b), 1 in c).

wt. %) content. There is a significant increase in the average Ta content in the cassiterite on the way from granite towards pegmatite type and a sharp decrease of Ta in the vein type (Fig. 6).

Figure 7 shows minor elements distributions within single cassiterite crystals. Spots were placed in different zones within single crystals as well across profiles from the crystal cores towards the rims. In general, concentrations of Fe, Nb and Ta increase in darkest zones of cassiterite whereas lightest zones are mostly depleted in minor/trace elements. In analysed crystals Ta/(Ta+Nb) ratio increases towards the crystal rim, although most of analysed crystals do not exhibit clear core to rim Ta–Nb chemical evolution pattern. Later generations of cassiter-

Tab. 1 Electron microprobe data on cassiterite in granite, quartz vein, pegmatite and greisen form Bugarura–Kuluti mining district.

	Granite cassiterite, 31 analyses				Vein cassiterite, 122 analyses				Pegmatite cassiterite, 285 analyses				Greisen cassiterite, 117 analyses			
	Av.	Min	Max	St. dev.	Av.	Min	Max	St. dev.	Av.	Min	Max	St. dev.	Av.	Min	Max	St. dev.
WO_3	0.01	bdl	0.11	0.03	0.01	bdl	0.09	0.02	0.01	bdl	0.13	0.03	0.02	bdl	0.24	0.03
Nb_2O_5	0.24	bdl	1.57	0.40	0.11	bdl	0.63	0.15	0.51	bdl	2.61	0.59	0.61	bdl	2.05	0.61
Ta_2O_5	0.54	bdl	3.83	0.89	0.12	bdl	0.94	0.17	1.41	bdl	14.24	1.92	1.26	bdl	5.54	1.19
TiO_2	0.13	bdl	0.54	0.19	0.46	0.12	1.05	0.14	0.07	bdl	0.65	0.14	0.02	bdl	0.39	0.05
ZrO_2	0.03	bdl	0.19	0.04	0.03	bdl	0.08	0.02	0.07	bdl	0.33	0.07	0.08	bdl	0.23	0.06
SnO_2	99.24	94.66	101.62	1.51	100.01	97.89	102.83	0.86	97.94	81.71	101.81	2.82	98.03	91.18	102.00	2.17
Al_2O_3	0.01	bdl	0.15	0.03	0.00	bdl	0.03	0.01	0.02	bdl	0.67	0.06	0.02	bdl	0.34	0.04
Sc_2O_3	0.00	bdl	0.02	0.00	0.01	bdl	0.04	0.01	0.01	bdl	0.04	0.01	0.01	bdl	0.04	0.01
In_2O_3	0.03	bdl	0.07	0.02	0.01	bdl	0.08	0.03	0.04	bdl	0.12	0.03	0.04	bdl	0.10	0.03
Sb_2O_3	0.00	bdl	0.05	0.01	0.00	bdl	0.09	0.01	0.00	bdl	0.09	0.01	0.01	bdl	0.07	0.02
MgO	0.04	bdl	0.09	0.03	0.04	bdl	0.10	0.02	0.03	bdl	0.10	0.02	0.02	bdl	0.08	0.02
CaO	0.06	bdl	1.77	0.31	0.03	bdl	0.25	0.06	0.04	bdl	0.85	0.08	0.02	bdl	0.12	0.03
MnO	0.04	bdl	0.39	0.08	0.01	bdl	0.06	0.01	0.05	bdl	0.43	0.08	0.02	bdl	0.20	0.03
FeO	0.10	bdl	0.53	0.13	0.05	bdl	0.21	0.05	0.29	bdl	2.49	0.34	0.33	bdl	1.49	0.28
ZnO	0.03	bdl	0.11	0.04	–	–	–	–	0.05	bdl	0.12	0.04	–	–	–	–
Total	100.50				100.88				100.56				100.59			
Chemical formula based on two oxygen atoms.																
W	0.000				0.000				0.000				0.000			
Nb	0.003				0.001				0.006				0.007			
Ta	0.004				0.001				0.010				0.009			
Ti	0.003				0.009				0.001				0.000			
Zr	0.000				0.000				0.001				0.001			
Sn	0.986				0.987				0.974				0.974			
Al	0.000				0.000				0.001				0.001			
Sc	0.000				0.000				0.000				0.000			
Sb	0.000				0.000				0.000				0.000			
Mg	0.001				0.002				0.001				0.001			
Ca	0.002				0.001				0.001				0.001			
Mn	0.001				0.000				0.001				0.001			
Fe	0.002				0.001				0.006				0.007			
Zn	0.000				0.000				0.000				0.000			
∑ cat.	1.002				1.001				1.001				1.001			

* bdl – below detection limit

ite are often marked by corroded texture, pale colours and significant amount of CGM inclusions (Fig. 7b, spots 4 and 5). Their chemical composition is characterised by the highest Ta/(Ta+Nb) and relatively low other minor elements.

The compositions of cassiterite from different types of host rocks were plotted on the (Nb,Ta)–(Fe,Mn)–(Sn,Ti) diagram (Figs 8a, b). The compositional trends defined by cassiterite crystals follow the ideal substitution $(Fe,Mn)^{2+} + 2(Nb,Ta)^{5+} = 3(Sn,Ti)^{4+}$ (Černý et al. 1985). This substitution is considered as the main mechanism responsible for the incorporation of Ti, Mn, Fe, and Nb into the studied cassiterite. Variations of Ti contents are observed in the Ti–Sn–(Nb,Ta) compositional diagram (Figs 8c, d). It shows high Ti content in the cassiterite from all quartz veins compared to cassiterite from pegmatites and greisens which shows high concentrations of Ta and Nb.

4.3. Inclusions of rutile and ilmenite in cassiterite

The rutile and ilmenite inclusions are rare and only occur in the cassiterite from hydrothermal quartz veins. The inclusions (40–100 μm in size) commonly occur in the fissures and cavities of cassiterite crystals. Rutile occurs as isolated phases and locally show intergrowth textures with ilmenite (Fig. 9a). Rarely,

Tab. 2 Electron microprobe data on rutile and two representative analyses of ilmenite inclusions in cassiterite form Bugarura–Kuluti mining district.

	Rutile									Ilmenite	
	1.	2.	3.	4.	5.	Av.	Min.	Max.	St.Dev.	1.	2.
WO_3	bdl	0.04	0.07	0.10	0.09	0.06	0.00	0.12	0.03	0.00	0.00
Nb_2O_5	6.90	13.49	11.86	4.81	7.89	7.06	0.25	13.49	3.93	0.14	0.19
Ta_2O_5	0.70	1.55	1.66	1.55	2.53	1.43	0.14	6.08	1.31	0.19	0.00
TiO_2	87.38	77.88	77.29	88.16	83.55	84.90	76.87	96.91	6.01	52.60	52.53
SnO_2	0.77	1.23	2.19	1.02	1.78	1.35	0.71	2.19	0.46	0.64	0.44
Sc_2O_3	0.03	0.04	bdl	bdl	bdl	0.01	0.00	0.04	0.01	0.00	0.00
Al_2O_3	0.07	0.08	0.27	0.20	0.17	0.17	0.02	0.28	0.08	0.01	0.00
Fe_2O_3	1.25	1.79	1.76	2.27	2.20	1.72	0.00	3.76	0.77		
FeO	1.38	3.00	2.38	0.23	1.32	1.22	0.00	3.00	0.97	43.63	43.06
MnO	bdl	bdl	0.04	bdl	bdl	0.01	0.00	0.04	0.02	1.97	3.16
Sum	98.48	99.08	97.68	98.33	99.52	97.93				99.18	99.38
	Formula based on cation sum = 1 and two oxygen atoms.									Formula based on 3 O atoms.	
W	0.000	0.000	0.001	0.001	0.001	0.000				0.000	0.000
Nb	0.044	0.088	0.078	0.030	0.050	0.046				0.002	0.002
Ta	0.003	0.006	0.007	0.006	0.010	0.006				0.001	0.000
Ti	0.919	0.842	0.849	0.927	0.887	0.905				1.005	1.002
Sn	0.004	0.007	0.013	0.006	0.010	0.008				0.006	0.004
Sc	0.000	0.001	0.000	0.000	0.000	0.000				0.000	0.000
Al	0.001	0.001	0.005	0.003	0.003	0.003				0.000	0.000
Fe^{3+}	0.013	0.019	0.019	0.024	0.023	0.018					
Fe^{2+}	0.016	0.036	0.029	0.003	0.016	0.015				0.927	0.913
Mn	0.000	0.000	0.001	0.000	0.000	0.000				0.042	0.068
∑ cat.	1.000	1.000	1.000	1.000	1.000	1.000				1.984	1.990

* FeO/Fe_2O_3 ratio was calculated at the basis of charge balance; bdl – below detection limit

Tab. 3 Representative electron-microprobe results of columbite-group minerals and tapiolite in the Bugarura–Kuluti district.

	Columbite-tantalite							Tapiolite	
	Pegmatite					Greisen		Pegmatite	
	1	2	3	4	5	1	2	1	2
WO_3	0.12	bdl	0.62	0.30	0.39	1.35	1.33	0.30	bdl
Nb_2O_5	25.81	27.80	38.35	25.17	18.19	45.22	45.44	6.42	5.06
Ta_2O_5	56.73	54.43	43.72	53.49	66.18	33.77	33.95	74.06	81.23
TiO_2	0.30	0.22	0.36	2.29	0.13	0.31	0.52	2.83	0.48
ZrO_2	0.08	0.44	bdl	0.17	0.04	bdl	0.10	0.14	0.04
SnO_2	0.21	0.44	0.13	1.58	0.13	0.16	0.23	1.41	0.68
Fe_2O_3	2.99	1.35	1.77	2.53	2.68	4.01	3.78	2.29	0.56
FeO	4.49	13.05	12.92	7.85	7.43	10.83	8.23	11.66	13.92
MnO	10.17	2.68	3.31	6.25	6.71	4.20	6.87	0.88	0.40
Total	100.90	100.40	101.19	99.63	101.88	99.17	100.54	99.99	102.38
	Formula based on three cations and six oxygen atoms.								
W	0.002	0.000	0.011	0.006	0.008	0.023	0.022	0.006	0.000
Nb	0.832	0.895	1.164	0.809	0.611	1.336	1.332	0.229	0.183
Ta	1.100	1.054	0.798	1.034	1.336	0.600	0.599	1.586	1.770
Ti	0.016	0.012	0.018	0.122	0.007	0.015	0.025	0.168	0.029
Zr	0.003	0.015	0.001	0.006	0.001	0.001	0.003	0.005	0.002
Sn	0.006	0.013	0.004	0.045	0.004	0.004	0.006	0.044	0.022
Fe^{3+}	160	0.072	0.090	0.136	0.150	0.197	0.184	0.136	0.034
Fe^{2+}	0.267	0.777	0.726	0.467	0.461	0.592	0.451	0.768	0.933
Mn	0.614	0.162	0.188	0.376	0.422	0.233	0.377	0.059	0.027
∑ cat.	3.000	3.000	3.000	3.000	3.000	3.000	3.000	3.000	3.000
Ta/(Ta+Nb)	0.6	0.5	0.4	0.6	0.7	0.3	0.3	0.9	0.9

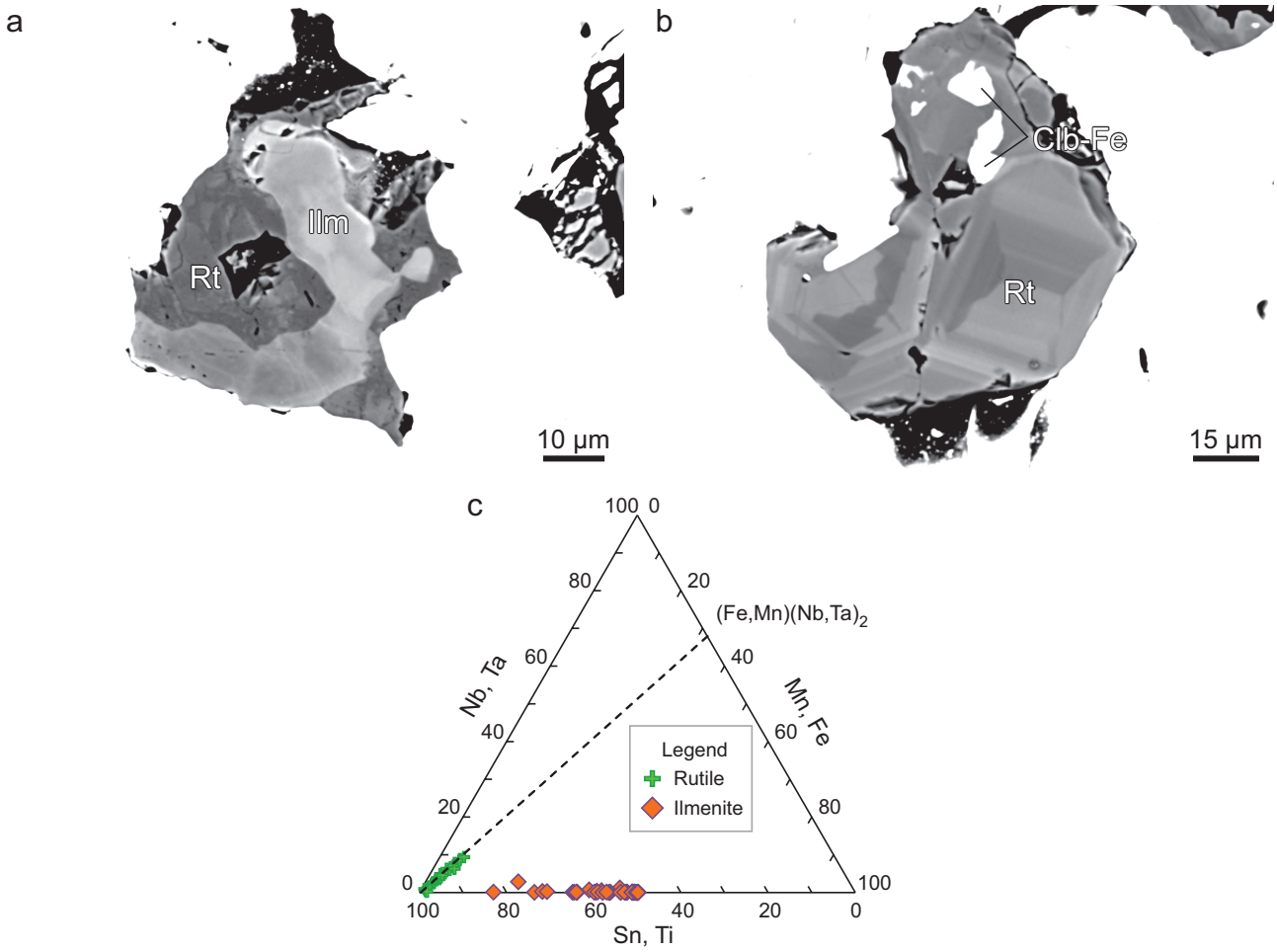

Fig. 9. BSE images of rutile and ilmenite (a-b) and (Na,Ta)–(Fe,Mn)–(Sn,Ti) composition diagram (c) for rutile and ilmenite occurring as inclusions in cassiterite from quartz vein deposits. Rt – rutile, Ilm – ilmenite, Clb-Fe – columbite-(Fe)

rutile host pure columbite-(Fe) inclusions (Fig. 9b). Rutile is irregularly, sector and oscillatory zoned, and reveals heterogeneous chemical composition (Tab. 2). Compositions of rutile and ilmenite inclusions were plotted in the (Nb,Ta)–(Fe,Mn) –(Sn,Ti) compositional diagram (Fig. 9c). Similarly to cassiterite, the main trend of rutile composition falls close to the ideal substitution $(Fe,Mn)^{2+}+2(Nb,Ta)^{5+}=3(Sn,Ti)^{4+}$ (Černý et al. 1985). In general, the substitution reaction in rutile from the BK deposit follows the $3Ti^{4+}\rightarrow Fe^{2+}+2Nb^{5+}$ scheme whereas ilmenite does not prefer to substitute Ta–Nb in its structure (Fig. 9c).

4.4. Inclusions of columbite–tantalite and tapiolite in cassiterite

Columbite group mineral (CGM) inclusions mainly occur in pegmatite and greisen types of cassiterite. They usually occur as small, black and red–black anhedral crystals in the brightest zones of the cassiterite (Figs 5b, c). CGM form (1) late euhedral species in cassiterite fractures and cavities (Figs 10a, c); (2) exsolution phases substituting cassiterite texture (Fig. 10b); and (3) subhedral to anhedral crystals filling fractures within cassiterite or cutting cassiterite crystals (Figs 10c, d). Most of CGM inclusions display oscillatory zoning characterised by periodic Nb- and Ta-rich zones (Fig. 10a). Tapiolite inclusions occur mostly in highly altered cassiterites from pegmatites.

Chemically, CGM inclusions varies depending on the type of host rock (Tab. 3). The Ta/(Ta+Nb) ratios of representative CGM inclusions in cassiterite from pegmatites range from 0.4 to 0.7 and are higher than those found in greisen cassiterite, reaching 0.3.

The composition of CGM inclusions was plotted in the Mn/(Mn+Fe) vs. Ta/(Ta+Nb) quadrilateral diagrams (Fig. 11). Generally, all studied CGM are enriched in Fe relative to Mn. CGM in greisen cassiterite is predominantly represented by columbite-(Fe), while CGM in pegmatite cassiterite plot from columbite-(Fe) through tantalite-(Fe) up to most evolved tapiolite-(Fe) (Fig. 11a). There are differences in fractionation trends of pegmatite- and greisen-type CGM (Fig. 11b). CGM inclusions from pegmatitic cassiterite show an increase in Ta/(Ta+Nb)

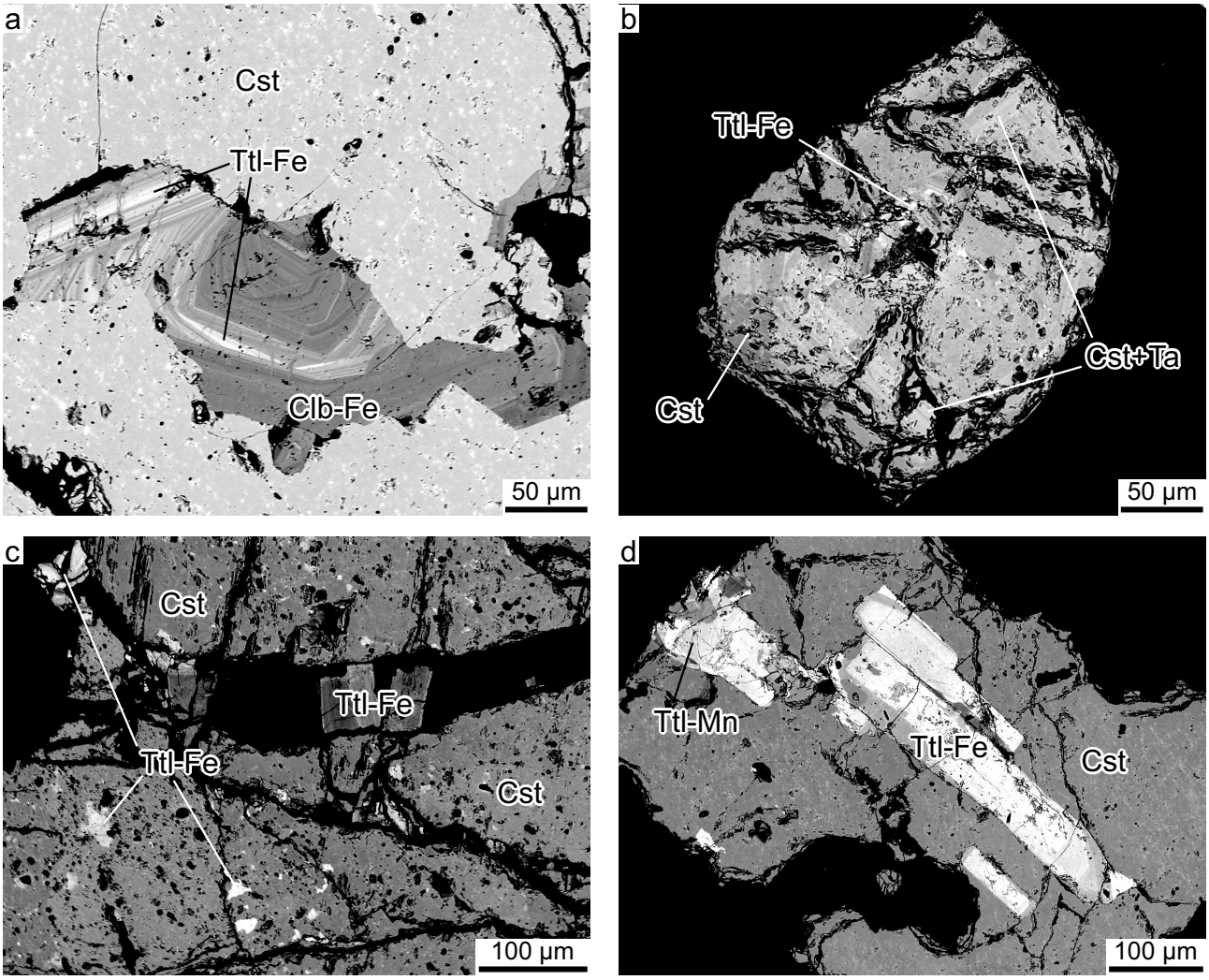

Fig. 10 BSE images of selected CGM inclusions. **a –** Oscillatory zoned CGM within greisen-type cassiterite. Bright zones are enriched in Ta, dark in Nb; **b –** exsolved CGM within cassiterite crystal from granitic pegmatite (Ttl-Fe). Lighter zones (Cst + Ta) represent cassiterite of high Ta_2O_5 content – up to 14 %; **c –** CGM inclusions in cassiterite from greisen. The tantalite-(Fe) crystallised within cassiterite crystal as well as in younger fractures; **d –** Euhedral to subhedral CGM crystals within cassiterite from pegmatite. Cst – cassiterite, Ttl-Fe – tantalite-(Fe), Ttl-Mn – tantalite-(MnFe), Clb-Fe – columbite-(Fe).

with increasing or decreasing Mn/(Mn + Fe) while CGM inclusions from greisen cassiterite show a decrease in Ta/(Ta + Nb) and Mn/(Mn + Fe).

5. Discussion

5.1. Tin in G4 granite

There are not known tin granites hosting economic amount of cassiterite in the Kibara Belt. Tin concentrations in the Rwandan granites G4 are between 4 and 80 ppm with an average of 19 ppm (Hulsbosch 2019). Heavy mineral concentrates from ~50 kg sample of the Muhazi G4 granite contained only few grains of cassiterite, which confirms the information from other parts of the Karagwe–Ankole Belt. On the other hand, there is fairly large amount of tourmaline (schorl) present, especially in the intragranitic pegmatites. Its presence is an indicator of boron saturation in the melt and its partitioning to the residual melt (Thomas et al. 2003).

The Muhazi G4 granite has no clearly developed greisen features. Some outer parts of the granite underwent only argillic alteration, probably due to circulating meteoric waters during late thermal events, not necessarily related to significant Sn mobilization. Trace amounts of cassiterite occur in the granite, which does not show signs of greisen development, suggesting its primary magmatic origin and crystallization directly from a melt in the granite and intragranitic pegmatites. Nevertheless, most of Sn partitioned into magmatic–hydrothermal fluids and escaped from solidifying granites. This was possible due to melt enrichment in H_2O, HCl and boron as a fluxing compound, lowering the viscosity and increasing its expansive features

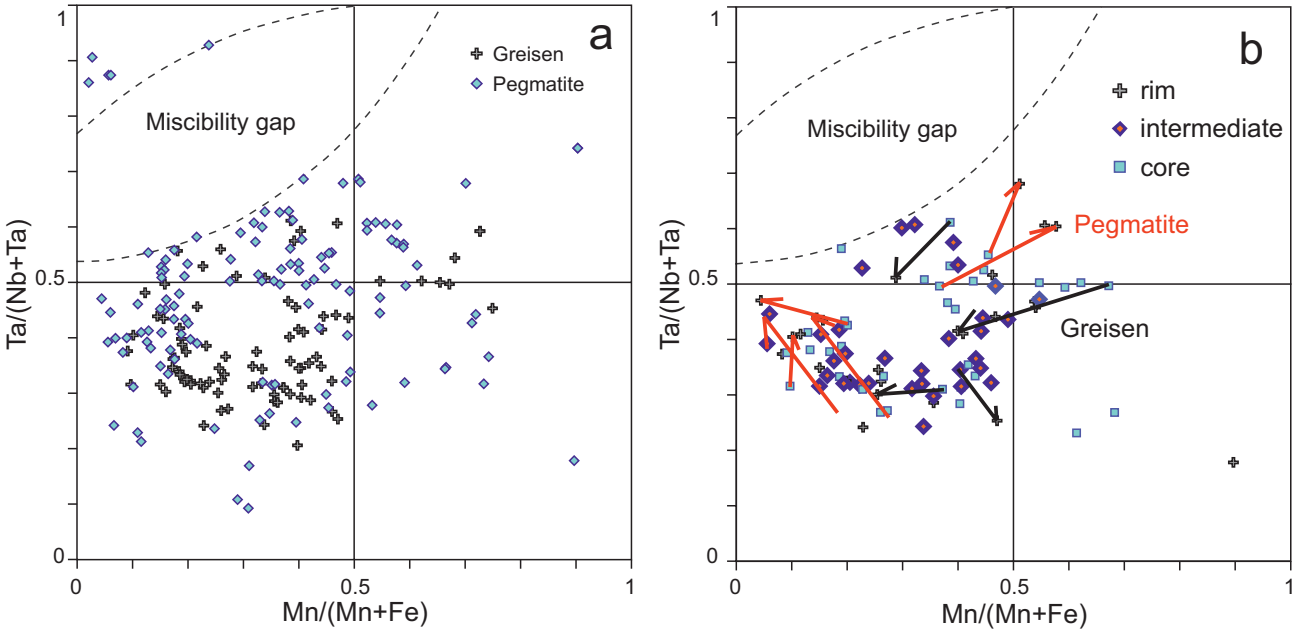

Fig. 11 Compositional (atom) ratios of CGM inclusions plotted in quadrilateral Mn/(Mn+Fe) vs. Ta/(Ta+Nb) diagrams (Černý and Ercit 1985). Diagram **(a)** distinguishes the compositions of inclusions from cassiterite hosted in greisen and pegmatite; diagram **(b)** shows fractionation trends based on individual crystals core–rim chemical composition for pegmatite and greisen. Most of the greisen CGM inclusions are columbite-(Fe). CGM inclusions in pegmatites have a more evolved geochemical signature and range in compositions from columbite-(Fe), tantalite-(Fe) to tapiolite-(Fe).

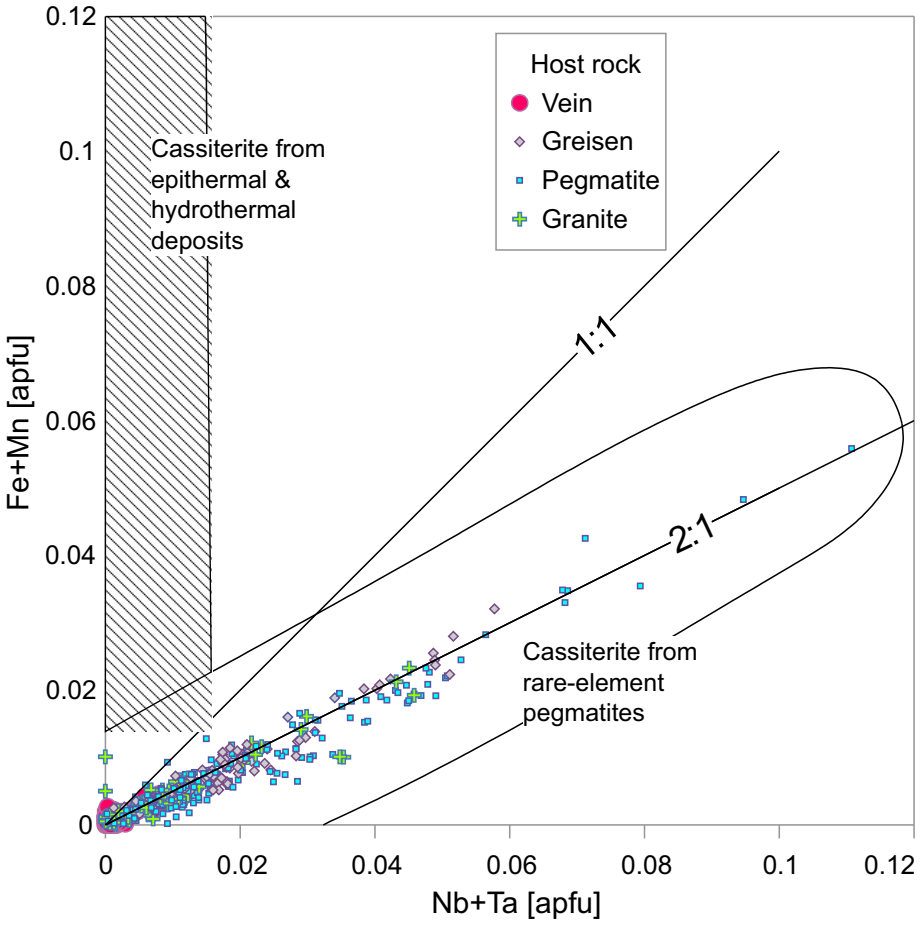

(Lehmann 1990). The most important parameter controlling Sn partitioning in hydrothermal fluids could have been high HCl concentration, which is a better Sn solvent than a felsic melt and NaCl or HF solutions (Duc-Tin et al. 2007; Schmidt 2018). Other relevant parameters are high temperature, low fO_2 and pH (Lehmann 1990).

Cassiterite from the granite has relatively low Ta and Ti concentrations. Ti is generally compatible and more susceptible to be incorporated in ilmenite, biotite, and other early crystallizing Ti-bearing minerals (Lehmann 2021), conversely to Ta which is

Fig. 12 Covariation of Fe+Mn vs. Nb+Ta for cassiterite from Bugarura and Kuluti deposits. The results indicate that origin of all studied cassiterites relates to rare-element pegmatites. Modified after Tindle and Breaks (1998).

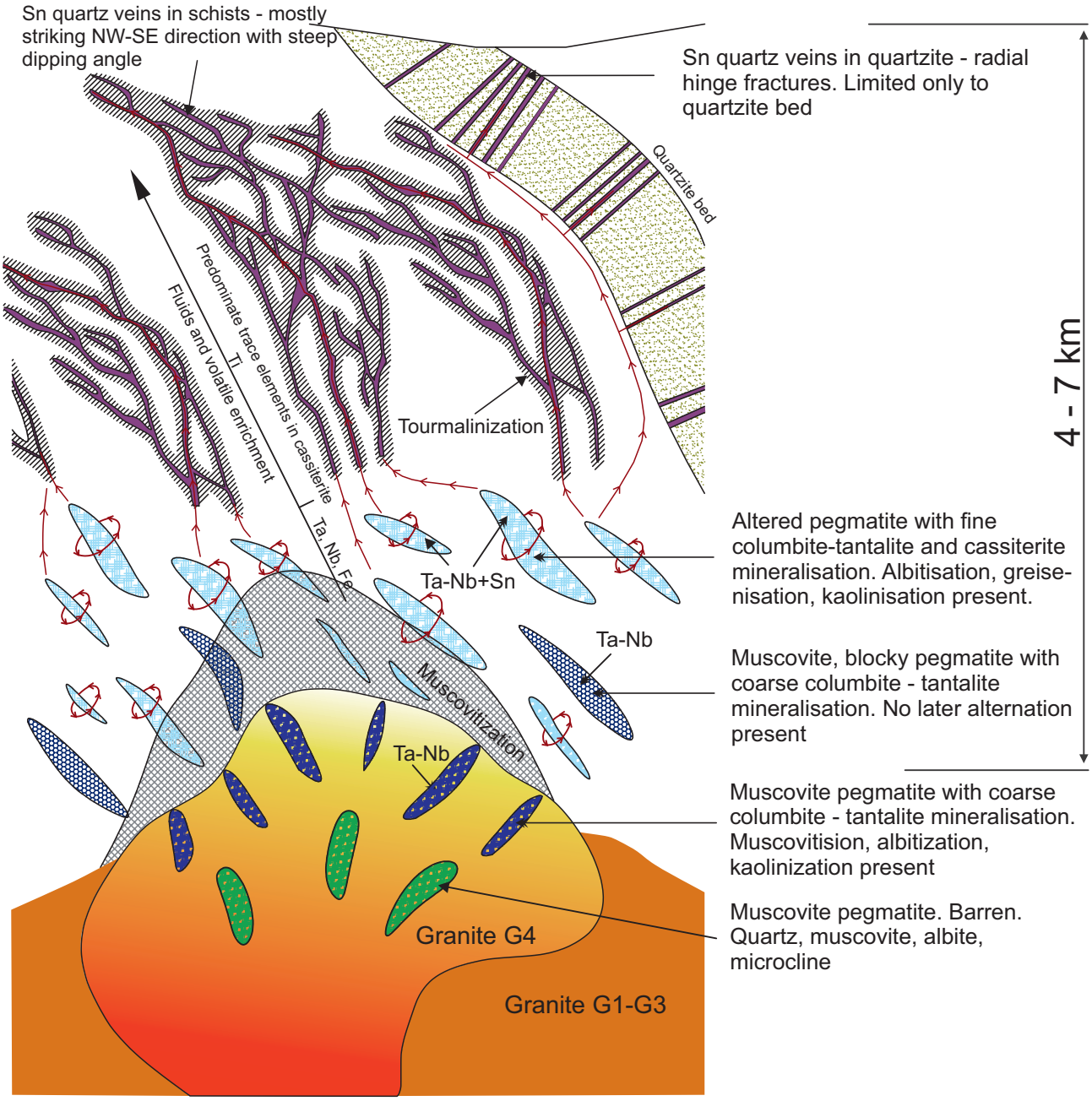

Fig. 13 Tin metallogenic model of Bugarura and Kuluti areas. Tin preferentially partitioned to fluid phases relative to the melts of G4 granite and percolated in metasedimentary country-rocks together with pegmatite melts. The fluid phases exsolved from solidifying pegmatites, altered their structure and precipitated Sn in greisens. Most of hydrothermal fluids escaped farther to sedimentary rocks where they reacted with the country rocks and meteoric water, precipitating quartz–muscovite veins with cassiterite.

incompatible and preferentially partitioned into residual melt. The concentrations of Ta in the Muhazi G4 granite vary from 0.6 ppm in the central part, to 1.6 ppm in the outer zone, whereas concentrations of Nb vary from 5.2 ppm to 13.2 ppm for the same zones (unpublished data). Such low concentrations hamper Ta and Nb incorporation into cassiterite and confirm incompatible nature in the early melt of these elements. The Fe+Mn vs. Ta+Nb diagram shows an affiliation of all types of cassiterite to rare element pegmatites (Fig. 12). Taking into consideration lack of later Sn quartz veins crossing pegmatites, we assume that pegmatitic melts were the source of Sn mineralising fluids.

5.2. Tin in pegmatites and greisens

The residual melt enriched in incompatible elements, volatiles and aqueous fluids escaped to the metasedimen-

tary suite to form LCT pegmatites. However, some parts of the residual melt remained in the granite, crystalizing as barren–muscovite pegmatites in the central part of the granite and CGM–muscovite pegmatites in the most apical part of the granitic intrusion (Fig. 13, Fig. 4b).

The pegmatite melt that escaped to the metasedimentary rock formations, stopped in structurally controlled traps where aqueous fluids, enriched in volatiles, exsolved from solidifying pegmatites. Hydrothermal fluids began to circulate in the system, altering newly-formed pegmatites (Fig. 13). Alteration of feldspars caused acid neutralisation and cassiterite crystallisation in the kaolinite–quartz–muscovite assemblage, and in the quartz–muscovite greisens (Reaction 1). The lack of fluorine-bearing minerals in greisen, and the presence of tourmalines in pegmatites, especially in the contact zones, confirms the boron-rich and F-poor character of the pegmatite melts. Following reaction can be considered (Hulsbosch 2019):

$$6KAlSi_3O_8 + [Sn(IV)Cl_3(H_2O)_3]^+ \leftrightarrow 2KAl_3Si_3O_{10}(OH)_2 + Sn(IV)O_2 + 12SiO_2 + K^+ + 3KCl^0 + H_2O$$

(i.e., 6 feldspar + fluid = 2 muscovite + cassiterite + 12 quartz + fluid) *Reaction 1*

Another possibility for tin (II) precipitation is a redox reaction involving H^+ consumption (Reaction 2). Nevertheless, both reactions are achievable by HCl reduction during feldspars alteration as follows (Hulsbosch 2019):

$$[Sn(II)Cl_x]H^{2-x} + 2H_2O \leftrightarrow Sn(IV)O_2 + 2H^+ + XCl^- + H_2$$ *Reaction 2*

A number of CGM inclusions in pegmatite cassiterites are likely a consequence of cassiterite precipitation from late-magmatic hydrosilicate fluids, which have both aqueous and silicate melt properties (Smirnov et al. 2012). Taking into consideration that Ta partitions preferentially into the melt till late-magmatic stage (Linnen and Keppler 1997), the existence of such solution could allow for undisturbed substitution $(Fe,Mn)^{2+} + 2(Nb,Ta)^{5+} = 3(Sn,Ti)^{4+}$ in cassiterite (Fig. 8). Some cassiterites may have precipitated directly from the pegmatite melt, which would also explain the numerous CGM inclusions (e.g., Linnen et al. 1996; Bhalla et al. 2005). The occurrence of euhedral CGM associated to greisen cassiterite indicate that some CGM precipitated from hydrothermal fluids during greisenization of pegmatites. Similar process has been observed in the Cape Cross–Uis pegmatite belt, Namibia (Fuchsloch et al. 2019).

The cassiterite from pegmatite and greisen has the lowest Ti concentrations, potentially due to early Ti incorporation in main and accessory minerals from the parental granite magma such as ilmenite and biotite (Tab. 1). Therefore, cassiterite was more susceptible to incorporate Ta and Nb over Ti in this environment. Moreover, a similar Ti concentration in greisen cassiterite compared to pegmatite cassiterite suggests that aqueous fluids exsolved from pegmatitic melt and did not underwent much interaction with country rocks. Lack of hydrothermal veins on the way from granite up to the pegmatites supports this observation.

Single pegmatites at a close distance to the granite were not all altered but still contain small amount of cassiterite (Fig. 4c). Apparently, the melts with low viscosity, rich in volatiles, aqueous fluids and majority of Sn, were able to move farther from the granite, leaving behind some of the undersaturated pegmatitic melt. The occurrence of cassiterite therefore indicates that the first generation of Sn was transported together with Ta and Nb in the residual melt and minority of tin precipitated directly from melts.

5.3. Tin in quartz veins

Hydrothermal veins were emplaced in the peripherical zone of the Bugarura–Kuluti metallogenic system. There is no evidence in the field for quartz veins crosscutting pegmatites, but field observations confirm transition zones from pegmatites to hydrothermal veins through greisen zones. These observations indicate that the mineralised fluids responsible for hydrothermal quartz veins were exsolved from the pegmatite melt rather than released directly form the granite as proposed for the Gatumba pegmatite fields in central Rwanda (Dewaele et al. 2008). Lack of CGM inclusions and low Ta and Nb concentrations in vein cassiterite (Tab. 1) suggest that hydrothermal fluids were not involved in the alteration of pegmatites. Instead, they escaped just after exsolving from the pegmatitic melt. The hydrothermal solutions transported tin out of the pegmatite melt farther to schists and quartzites using tectonic pathways. Due to the fluid interaction with country rocks, cassiterite precipitated in hydrothermal quartz veins. Two reactions have been proposed for this process; both absorbing Cl^- from hydrothermal $Sn^{2+}Cl^-$ complex (Hulsbosch 2019; Nambaje et al. 2020). First, acid consumption by fluid interaction with felspars in sandstones–quartzites leading to muscovitization and cassiterite precipitation (Reaction 1) (Hulsbosch 2019). Second, acid consumption by fluid interaction with biotite in schists leading to the same main products (Reaction 3) (Nambaje et al. 2020):

$$3KFe_3AlSi_3O_{10} + 20HCl \leftrightarrow KAl_3Si_3O_{10}(OH)_2 + 6SiO_2 + 9FeCl_2 + 2KCl + 12H_2O$$

(biotite) *(muscovite)* *(quartz)* *Reaction 3*

The $\delta^{18}O$ and δD stable isotope analysis of quartz and cassiterite from mineralised quartz veins indicated cassiterite precipitation during metamorphic hydrothermal conditions (Dewaele et al. 2010). However, later studies led to the conclusion that magmatic hydrothermal fluids mixed with meteoric water after separation from the melt (Van Daele et al. 2018). The internal zoning of veins composed of muscovite selvage with cassiterite and quartz core, support fluid–rock interaction (Fig. 4g). Hydrothermal fluids interacted with feldspar and/or biotite producing muscovite together with cassiterite on the contact with country rock whereas quartz precipitated as the last in the core of the vein. Zoned veins were observed only in schists which more preferably interacted with hydrothermal solutions and at the same time are less permeable than quartzites hampering mixing of magmatic and meteoric fluids. The wall-rock interaction process is also supported by increased Ti concentration in cassiterite, which was released from country rocks to the hydrothermal system (Tab. 1). Unzoned veins occur in both schist and quartzite hosting rocks and in addition, they do not show presence of muscovite-rich layers. The muscovite crystallised randomly within quartz together with cassiterite and iron oxides/hydroxides (Fig. 4h). Quartzites in Bugarura–Kuluti area, which host only unzoned veins, do not contain feldspar and biotite which could support fluid–wall rock reaction. However, increased permeability through hinge extensional fractures promoted magmatic–meteoric fluid mixing which is reflected by metamorphic signature of fluid inclusions (Dewaele et al. 2010).

5.4. Younger thermal events

In the Bugarura–Kuluti deposit, microscopic observations confirm later cassiterite generations in all studied deposits (Figs 5b, d). In greisen and pegmatites, late cassiterite generations occur as almost transparent phases with numerous CGM inclusions (Fig. 5b). They often form corroded, dissolution–reprecipitation textures on edges of cassiterite crystals (Figs 7b, c). The highest Ta/(Ta + Nb) ratio in these zones and a high number of CGM inclusions possibly indicate new magma pulses or decreasing temperature of the system that could involve magmatic–hydrothermal transition. New magma patches could alter also primary CGM crystals, which has been also observed in the Bugarura–Kuluti area (Ryznar et al. 2023). There are also single cassiterite bounds enriched in CGM inclusions, suggesting that these inclusions were captured by cassiterite during crystal growth. Such phenomena could possibly confirm magma pulses. The change of magmatic–hydrothermal system condition and possible repetition of a hydrothermal/magmatic activity is confirmed by at least three different types of fluid inclusions in cassiterite from hydrothermal quartz veins (Pohl and Günther 1991) and from pegmatites (Hulsbosch and Muchez 2020). The change in cassiterite generations are not visible in CL images, also the change of chemical composition is not significant. Therefore, we conclude that the younger generations were formed during a single magmatic event as a result of dissolution–reprecipitation processes, rather than younger thermal reactivation of the BK magmatic/hydrothermal system.

In a regional scale, there are verity in styles of Ta–Nb–W–Sn deposits in different locations of the Kibara Belt. For example, the Rwinkwavu (eastern Rwanda) and Kyerwa (northwestern Tanzania) tin deposits located to the east from the BK developed only quartz veins with Sn–W mineralisation while Muhanga and Kamonyi districts in the central part of Rwanda are chiefly known for the occurrence of pegmatites with Ta–Nb–Sn mineralisation. Such diversity is not only a matter of differentiation of granitic melt but also different timing of emplacement (e.g., Pohl 1994; Nambaje et al. 2021). The most recent work on Rwandan granites indicates their anatectic origin in intracontinental setting (De Clercq et al. 2021). It is considered that the melting was very localised. It involved different amount of crustal and sedimentary material which had an impact on melts differentiation and consequently, on the diverse composition of granites. Such diversity may explain different styles of Ta–Nb–W–Sn deposits in different locations of Kibara Belt. Another factor is the timing, the G4 magmatic event at ~1 Ga is the only period known for pegmatites emplacement in the area (e.g., Pohl 1994; Dewaele et al. 2010; Hulsbosch 2019). Younger events resulted only in hydrothermal quartz veins emplacement with cassiterite (Nambaje et al. 2021). To explain this phenomenon a more regional research on the younger granites is needed.

6. Conclusions

1. The cassiterite from the Bugarura–Kuluti mining district is related to the G4 Muhazi granite. It occurs in hydrothermal quartz–muscovite veins, LCT pegmatites, greisens and as traces in the G4 parental granite.
2. Depending on the type of deposit, the cassiterite displays variation in micro-texture, mineral inclusions and chemical composition. The size of cassiterite crystals increases away from the granite (~1 mm in pegmatite, ~10 mm in greisen and ~5 cm in quartz vein). The cassiterite from pegmatites and greisen contains numerous Nb–Ta oxide inclusions. It displays high Fe, Nb and Ta contents and low Ti concentrations. The cassiterite from hydrothermal quartz veins hosts rutile and ilmenite inclusions and has high Ti concentration.

3. The trace element incorporation in the cassiterite is described chiefly by the substitution: $(Fe,Mn)^{2+} + 2(Nb,Ta)^{5+} = 3(Sn,Ti)^{4+}$.
4. The origin of hydrothermal fluids with tin mineralisation from the Bugarura–Kuluti is strongly related to rare-element pegmatites, which is confirmed by the positive correlation between Fe + Mn and Nb + Ta.
5. In the Bugarura and Kuluti area, Sn was possibly extracted from the melt by magmatic–hydrothermal solutions as chloride complexes. These solutions were moved to metasedimentary rocks and trapped in tectonic fractures. First cassiterite precipitated from the melt and possibly hydrosilicate fluids where it incorporated elements which reluctantly partition to aqueous fluids (e.g., Ta). During progressing fractionation, aqueous fluids enriched in volatiles exsolved from the residual magma and started circulating in the newly created pegmatite, altering feldspars and precipitating cassiterite in greisens and kaolinite–quartz–muscovite assemblages.
   Most of the exsolved fluids escaped to metasedimentary rocks where they could interact with country rocks and/or mix with meteoric water. The fluid–rock interaction resulted in zoned quartz veins with muscovite selvages while fluids mixing resulted in unzoned veins in quartzites and schists.
6. Younger cassiterite generations are formed in a process of dissolution–reprecipitation of earlier mineralisations during changing system conditions.

Acknowledgements. The research is funded by a doctoral fellowship of the Ministry of Science and Higher Education and significant support of prof. Radoslaw Miskiewicz. Authors thank LuNa Smelter Ltd for the access to their concession, substantial support in samples preparation and laboratory assistance. The Rwanda government is thanked for the export authorisation of samples. Thomas Tumukunde is thanked for all the support during field work. We appreciate the constructive and insightful comments by the reviewers Christophe Ballouard and Milan Novák.

Electronic supplementary material. Supplementary table of EMPA Raw data is available online at the Journal web site (*http://dx.doi.org/10.3190/jgeosci.389*).

References

Baudet D, Hanon M, Lemonne E, Theunissen K, Buyagu S, Dehandschutter J, Ngizimana W, Nsengiyumva P, Rusanganwa JB, Tahon A (1988) Lithostratigraphie du domaine sédimentaire de la chaîne Kibarienne au Rwanda. Annales Soc géol Belg 112: 225–246

Bhalla P, Holtz F, Linnen RL, Behrens H (2005) Solubility of cassiterite in evolved granitic melts: Effect of *T*, *f*O2, and additional volatiles. Lithos 80: 387–400

Černý P, Ercit TS (2005) The classification of granitic pegmatites. Canad Mineral 43: 2005–2026

Černý P, Roberts WL, Ercit TS, Chapman R (1985) Wodginite and associated oxide minerals from the Perless pegmatite, Pennington County, South Dakota. Amer Miner 70: 1044–1049

Cheng Y, Spandler C, Kemp A, Mao J, Rusk B, Hu Y, Blake K (2019) Controls on cassiterite (SnO_2) crystallization: Evidence from cathodoluminescence, trace-element chemistry, and geochronology at the Gejiu Tin District. Amer Miner 104: 118–129

Debruyne D, Hulsbosch N, Van Wilderode J, Balcaen L, Vanhaecke F, Muchez P (2015) Regional geodynamic context for the Mesoproterozoic Kibara Belt (KIB) and the Karagwe–Ankole Belt: Evidence from geochemistry and isotopes in the KIB. Precambr Res 264: 82–97

De Clercq S, Chew D, O'sullivan G, De Putter T, De Grave J, Dewaele S (2021) Characterisation and geodynamic setting of the 1 Ga granitoids of the Karagwe–Ankole belt (KAB), Rwanda. Precambr Res 356: 106124

Dewaele S, Tack L, Fernandez-Alonso M, Boyce A, Muchez P, Schneider J, Cooper G, Wheeler K (2008) Geology and mineralisation of the Gatumba area, Rwanda: present state of knowledge. Etudes Rwandaises 16: 6–24

Dewaele S, Clercq F, Muchez P, Schneider J, Burges SR, Boyce A, Fernandez-Alonso M (2010) Geology of the cassiterite mineralisation in the Rutongo area, Rwanda (Central Africa): Current state of knowledge. Geol Belg 13: 91–112

Dewaele S, Henjes-Kunst F, Melcher F, Sitnikova M, Burgess R, Gerdes A, Fernandez-Alonso M, Clercq F, Muchez P, Lehmann B (2011) Late Neoproterozoic overprinting of the cassiterite and columbite–tantalite bearing pegmatites of the Gatumba area, Rwanda (Central Africa). J Afr Earth Sci 61: 10–26

Dewaele S, Hulsbosch N, Cryns Y, Boyce A, Burgess R, Muchez P (2016) Geological setting and timing of the world-class Sn, Nb–Ta and Li mineralisation of Manono-Kitotolo (Katanga, Democratic Republic of Congo). Ore Geol Rev 72: 373–390

Duc-Tin Q, Audétat A, Keppler H (2007) Solubility of tin in (Cl, F)-bearing aqueous fluids at 700 °C, 140 MPa: a LA-ICP-MS study on synthetic fluid inclusions. Geochim Cosmochim Acta 71: 3323–3335

Fernandez-Alonso M, Cutten H, De Waele B, Tack L, Tahon A, Baudet D, Barritt SD (2012) The Mesoproterozoic Karagwe–Ankole Belt (formerly the NE Kibara Belt): The result of prolonged extensional intracratonic basin development punctuated by two short-lived far-field compressional events. Precambr Res 216–219: 63–86

Fuchsloch W, Nex P, Kinnaird J (2019) The geochemical evolution of Nb–Ta–Sn oxides from pegmatites of the Cape Cross–Uis pegmatite belt, Namibia. Mineral Mag 83: 161–179

Hanon M, Rusanganwa JB (1991) Carte géologique du Rwanda , Feuille Kigali (1 : 100,000). Département de Géologie et de Minéralogie du Musée Royal de l'Afrique Centrale et le Ministére de l'industrie et de l'Artisanat du Rwanda

Hulsbosch N (2019) Nb–Ta–Sn–W distribution in granite-related ore systems: fractionation mechanisms and examples from the Karagwe–Ankole Belt of Central Africa. In: Decrée S, Robb L (eds) Ore Deposits: Origin, Exploration, and Exploitation, Geophysical Monograph 242. John Wiley & Sons, pp 75–107

Hulsbosch N, Muchez P (2020) Tracing fluid saturation during pegmatite differentiation by studying the fluid inclusion evolution and multiphase cassiterite mineralisation of the Gatumba pegmatite dyke system (NW Rwanda). Lithos 354–355: 105285

Hulsbosch N, Hertogen J, Dewaele S, André L, Muchez P (2013) Petrographic and mineralogical characterisation of fractionated pegmatites culminating in the Nb–Ta–Sn pegmatites of the Gatumba area (western Rwanda). Geol Belg 16: 105–117

Hulsbosch N, Van Daele J, Reinders N, Dewaele S, Jacques D, Muchez P (2017) Structural control on the emplacement of contemporaneous Sn–Ta–Nb mineralised LCT pegmatites and Sn bearing quartz veins: Insights from the Musha and Ntunga deposits of the Karagwe–Ankole Belt, Rwanda. J Afr Earth Sci 134: 24–32

Kokonyangi J, Armstrong R, Kampunzu AB, Yoshida M, Okudaira T (2004) U–Pb zircon geochronology and petrology of granitoids from Mitwaba (Katanga, Congo): implications for the evolution of the Mesoproterozoic Kibaran belt. Precambr Res 132: 79–106

Lehmann B (2021) Formation of tin ore deposits: A reassessment. Lithos 402–403: 105756

Lehmann B (1990) Metallogeny of Tin. Springer Berlin, Heidelberg

Linnen RL, Keppler H (1997) Columbite solubility in granitic melts: consequences for the enrichment and fractionation of Nb and Ta in the Earth's crust. Contrib Mineral Petrol 128: 213–227

Linnen RL, Pichavant M, Holtz F (1996) The combined effects of *f*O2 and melt composition on SnO_2 solubility and tin diffusivity in haplogranitic melts. Geochim Cosmochim Acta 60: 4965–4976

Melcher F, Graupner T, Gäbler HE, Sitnikova M, Henjes-Kunst F, Oberthür T, Gerdes A, Dewaele S (2015) Tantalum–(niobium–tin) mineralisation in African pegmatites and rare metal granites: Constraints from Ta–Nb oxide mineralogy, geochemistry and U–Pb geochronology. Ore Geol Rev 64: 667–719

Möller P, Dulski P, Szacki W, Malow G, Riedel E (1988) Substitution of tin in cassiterite by tantalum, niobium, tungsten, iron and manganese. Geochim Cosmochim Acta 52: 1497–1503

Moscati RJ, Neymark LA (2020) U–Pb geochronology of tin deposits associated with the Cornubian Batholith of southwest England: Direct dating of cassiterite by in situ LA-ICPMS. Mineral Depos 55: 1–20

Nambaje C, Eggins S, Yaxley G, Sajeev K (2020) Microcharacterisation of cassiterite by geology, texture and zonation: A case study of the Karagwe–Ankole Belt, Rwanda. Ore Geol Rev 124: 103609

Nambaje C, Williams I, Sajeev K (2021) SHRIMP U–Pb dating of cassiterite: Insights into the timing of Rwandan tin mineralisation and associated tectonic processes. Ore Geol Rev 135: 104185

Pieczka A, Gołębiowska B, Parafiniuk J (2007) Geochemistry and origin of the cassiterite from Redziny, Lower Silesia, Poland. Mineralogia 38: 219–230

Pohl W (1994) Metallogeny of the northeastern Kibara belt, Central Africa: Recent perspectives. Ore Geol Rev 9: 105–130

Pohl W, Günther MA (1991) The origin of Kibaran (late Mid-Proterozoic) tin, tungsten and gold quartz vein deposits in Central Africa: a fluid inclusions study. Mineral Depos 26: 51–59

Pohl WL, Biryabarema M, Lehmann B (2013) Early Neoproterozoic rare metal (Sn, Ta, W) and gold metallogeny of the Central Africa Region: a review. Appl Earth Sci 122: 66–82

Rusanganwa JB (1988) Stratigraphie du Burundien au Rwanda. International References 265 Geological Correlation Programme, Project no. 255. TU Braunschweig-MRAC Tervuren, 1, 51–53

Ryznar J, Prsek J, Włodek A, Uher P (2023) Mineralogy and chemistry of columbite–tantalite from Bugarura–Kuluti area, Karagwe–Ankole Belt, Rwanda: indicators of pegmatite and granite evolution. Ore Geol Rev 159: 105574

Schmidt C (2018) Formation of hydrothermal tin deposits: Raman spectroscopic evidence for an important role of aqueous Sn(IV) species. Geochim Cosmochim Acta 220: 499–511

Schneider HJ, Dulski P, Luck J, Moeller P, Villalpando A (1978) Correlation of trace element distribution in cassiterites and geotectonic position of their deposits in Bolivia. Mineral Depos 13: 119–122

Smirnov SZ, Thomas VG, Kamenetsky VS, Kozmenko OA, Large RR (2012) Hydrosilicate liquids in the system Na_2O–SiO_2–H_2O with NaF, NaCl and Ta: Evaluation of their role in ore and mineral formation at high T and P. Petrology 20: 271–285

Tack L, Wingate MTD, De Waele B, Meert J, Belousova E, Griffin B, Tahon A, Fernandez-Alonso M

(2010) The 1375Ma "Kibaran event" in Central Africa: Prominent emplacement of bimodal magmatism under extensional regime. Precambr Res 180: 63–84

Thomas R, Förster HJ, Heinrich W (2003) The behaviour of boron in peraluminous granite–pegmatite systems and associated hydrothermal solutions: a melt and fluid inclusion study. Contrib Mineral Petrol 144: 457–472

Tindle AG, Breaks FW (1998) Oxide minerals of the separation rapids rare-element granitic pegmatite group, Northwestern Ontario. Canad Mineral 36: 609–635

Van Daele J, Hulsbosch N, Dewaele S, Boiron MC, Piessens K, Boyce A, Muchez P (2018) Mixing of magmatic–hydrothermal and metamorphic fluids and the origin of peribatholitic Sn vein-type deposits in Rwanda. Ore Geol Rev 101: 481–501

Van Daele J, Hulsbosch N, Dewaele S, Muchez P (2020) Metamorphic and metasomatic evolution of the Western Domain of the Karagwe–Ankole Belt (Central Africa). J Afr Earth Sci 165: 103783

Varlamoff N (1972) Central and West African rare-metal granitic pegmatites, related aplites, quartz veins and mineral deposits. Mineral Depos 7: 202–216

Zoheir B, Lehmann B, Emam A, Radwan A, Zhang R, Bain W M, Steele-Macinnis M, Nolte N (2020) Extreme fractionation and magmatic–hydrothermal transition in the formation of the Abu Dabbab rare-metal granite, Eastern Desert, Egypt. Lithos 352–353: 105329